

## Alfvénic Turbulence in the Extended Solar Corona: Kinetic Effects and Proton Heating

S. R. Cranmer and A. A. van Ballegoijen

*Harvard-Smithsonian Center for Astrophysics, 60 Garden Street, Cambridge, MA 02138*

### ABSTRACT

We present a model of magnetohydrodynamic (MHD) turbulence in the extended solar corona that contains the effects of collisionless dissipation and anisotropic particle heating. Recent observations have shown that preferential heating and acceleration of positive ions occurs in the first few solar radii of the high-speed solar wind. Measurements made by the Ultraviolet Coronagraph Spectrometer aboard *SOHO* have revived interest in the idea that ions are energized by the dissipation of ion cyclotron resonant waves, but such high-frequency (i.e., small wavelength) fluctuations have not been observed. A turbulent cascade is one possible way of generating small-scale fluctuations from a pre-existing population of low-frequency MHD waves. We model this cascade as a combination of advection and diffusion in wavenumber space. The dominant spectral transfer occurs in the direction perpendicular to the background magnetic field. As expected from earlier models, this leads to a highly anisotropic fluctuation spectrum with a rapidly decaying tail in the parallel wavenumber direction. The wave power that decays to high enough frequencies to become ion cyclotron resonant depends on the relative strengths of advection and diffusion in the cascade. For the most realistic values of these parameters, though, there is insufficient power to heat protons and heavy ions. The dominant oblique fluctuations (with dispersion properties of kinetic Alfvén waves) undergo Landau damping, which implies strong parallel electron heating. We discuss the probable nonlinear evolution of the electron velocity distributions into parallel beams and discrete phase-space holes (similar to those seen in the terrestrial magnetosphere) which can possibly heat protons via stochastic interactions.

*Subject headings:* MHD — plasmas — solar wind — Sun: corona — turbulence — waves

### 1. Introduction

In order to produce the hot ( $10^6$  K) solar corona, a fraction of the mechanical energy in the Sun's internal convective motions must be converted into heat above the photosphere. Despite more than a half century of investigation, though, the precise physical processes that lead to coronal heating and the subsequent acceleration of the solar wind are not known. At the coronal base, different combinations of mechanisms (e.g., magnetic reconnection, turbulence, wave dissipation, and plasma instabilities) are probably responsible for the varied ap-

pearance of coronal holes, quiet regions, loops, and X-ray bright points (Priest et al. 2000). In the open magnetic flux tubes that feed the solar wind, additional heating at heliocentric distances greater than about 2 solar radii ( $R_{\odot}$ ) is believed to be needed (e.g., Leer, Holzer, & Flå 1982; Parker 1991). This paper investigates the consequences of a promising mechanism for extended coronal heating: the kinetic dissipation of driven magnetohydrodynamic (MHD) turbulence in the strong background magnetic field of the accelerating solar wind.

The necessity for gradual energy deposition at large distances from the coronal base comes from three sets of empirical constraints (see also Cranmer 2002). First, pressure-driven models of the high-speed component ( $v \gtrsim 750 \text{ km s}^{-1}$ ) of the solar wind cannot be made consistent with the relatively low inferred electron temperatures in coronal holes ( $T_e < 1.5 \times 10^6 \text{ K}$ ) without additional energy or momentum deposition. Second, spacecraft in the interplanetary medium have measured radial gradients in proton and electron temperatures that are substantially shallower than predicted from pure adiabatic expansion (Phillips et al. 1995; Richardson et al. 1995). Similar measurements of radial growth of the proton magnetic moment between the orbits of Mercury and the Earth (Schwartz & Marsch 1983; Marsch 1991) point to specific forms of gradual energy addition. Third, the Ultraviolet Coronagraph Spectrometer (UVCS) aboard the *Solar and Heliospheric Observatory (SOHO)* measured extremely high heavy ion temperatures, faster bulk ion outflow compared to protons, and strong anisotropies (with  $T_{\perp} \gg T_{\parallel}$ ) in ion velocity distributions in the extended corona (Kohl et al. 1997, 1998, 1999; Noci et al. 1997; Cranmer et al. 1999b; Giordano et al. 2000).

The list of possible physical processes responsible for extended coronal heating is limited severely by the fact that Coulomb collisions are extremely weak above 2 to 3  $R_{\odot}$  and that ions receive more energy than electrons (with  $T_{\text{ion}} \gg T_p \gtrsim T_e$ ). Also, most suggested mechanisms involve the transfer of energy from propagating fluctuations—such as waves, shocks, or turbulent eddies—to the particles. This broad consensus has arisen because the ultimate source of energy must be solar in origin, and thus it must somehow be transmitted out to the distances where the heating occurs (see, e.g., Hollweg 1978; Tu & Marsch 1995). The most common wave damping mechanisms proposed for the coronal base (resistivity, viscosity, and thermal conductivity) seem to be ruled out in the extended corona because of the relative unimportance of collisions.

Wave-particle interactions are natural alternatives to collisional processes and have been studied in a solar wind context for several decades (Barnes 1968; Toichi 1971; Abraham-Shrauner & Feldman 1977; Hollweg & Turner 1978; Marsch, Goertz, & Richter 1982; Isenberg & Hollweg 1983; Hollweg 1986; Tu 1987, 1988; Axford & McKenzie 1992). The *SOHO* observations dis-

cussed above have given rise to a resurgence of interest in the collisionless dissipation of ion cyclotron waves as a potentially important mechanism in the acceleration region of the high-speed wind (e.g., McKenzie et al. 1995; Tu & Marsch 1997, 2001; Hollweg 1999b; Li et al. 1999; Galinsky & Shevchenko 2000; Cranmer 2000, 2001, 2002; Hollweg & Isenberg 2002; Vocks & Marsch 2002). In the extended corona, the cyclotron or Larmor frequencies of positive ions range from 10 to  $10^4 \text{ Hz}$ , but the oscillation frequencies observed on the solar surface (dominated by convection) are typically  $\sim 0.01 \text{ Hz}$ . Thus, any wave generation mechanism seems to require bridging a gap of many orders of magnitude in frequency or wavenumber.

Axford & McKenzie (1992) suggested that high-frequency Alfvén waves could be generated during small-scale reconnection events in the rapidly evolving supergranular network. These waves would propagate up through the corona until they reach the cyclotron resonance radii of various ions, then damp over a very short distance (see also Schwartz, Feldman, & Gary 1981). Tu & Marsch (1997) and Marsch & Tu (1997) presented solar wind models based on the idea that a launched power spectrum becomes “swept up” and eroded by the slow radial decrease of the cyclotron frequency. The general scenario of cyclotron sweeping has been called into question by Cranmer (2000), Hollweg (2000), and Leamon et al. (2000), but its relative importance in relation to other physical processes has not yet been fully established (see also Tu & Marsch 2001).

Alternatively, there have been numerous “local” wave generation scenarios proposed that involve the transfer of energy from other sources into the ion cyclotron mode at a range of heights in the acceleration region of the solar wind. Into this class of models fall the processes of MHD turbulent cascade, kinetic plasma instabilities (driven by non-Maxwellian velocity distributions or spatial gradients), or wave mode conversion driven by reflection or refraction (e.g., Hollweg 1986; Matthaeus et al. 1999; Kaghshvili & Esser 2000; Markovskii 2001; Moran 2002). Most of these local wave generation models rely on the Sun launching a sufficiently intense spectrum of low-frequency (i.e., with periods longer than  $\sim 5 \text{ min}$ ) Alfvén or fast-mode MHD waves that do not damp within a solar radius of the surface. At present, however, there are few empirical constraints on the gener-

ation mechanisms, exact propagation modes, or power levels of ion cyclotron waves in the corona.

In this paper we study the consequences of anisotropic MHD turbulent cascade as a possible generation mechanism for ion cyclotron waves in the extended corona. We also examine the turbulent cascade as a source of other forms of energy—such as parallel electron beams and phase-space holes—that could also lead to ion heating in the corona. We model the cascade as a diffusion process in three-dimensional wavenumber space and recover the basic form of the Goldreich & Sridhar (1995) spectral anisotropy. This solution for the turbulent power spectrum is coupled to a general Alfvén wave dispersion relation in order to compute the relative amounts of heating given to protons and electrons. The dispersive properties of the highly oblique kinetic Alfvén wave (KAW; see Stéfant 1970; Hasegawa 1976; Lysak & Lotko 1996; Hollweg 1999a; Stasiewicz et al. 2000) turn out to be key drivers of the plasma conditions of the extended corona. The KAW has been studied in a coronal and solar wind context by Dobrowolny & Torricelli-Ciamponi (1985), Song (1996), Leamon et al. (1998, 1999, 2000), Shukla et al. (1999), and Voitenko & Goossens (2002).

The remainder of this paper is organized as follows. In § 2 we develop a semianalytical model of anisotropic MHD turbulence by extending the wavenumber diffusion picture of Zhou & Matthaeus (1990) to three dimensions. In § 3, proton and electron heating rates that are consistent with the derived power spectrum are computed from a Vlasov-Maxwell kinetic dispersion relation. For the realistic case that KAWs heat electrons in the direction parallel to the magnetic field, § 4 follows a speculative chain of reasoning that leads to the generation of electron phase-space holes (EPHs) that can heat protons and heavy ions via Coulomb-like collisions. Conclusions, remaining questions, and implications for future spectroscopic observations are summarized in § 5.

## 2. Turbulent Cascade in the Extended Corona

In this section we derive the Fourier power spectrum of turbulent Alfvénic fluctuations as a function of the wavevector  $\mathbf{k}$  in the low plasma-beta extended corona. We assume that the turbulence is driven at

large scales by waves that originate at the Sun, and that some process (such as reflection) generates inward-propagating waves to excite a cascade (Matthaeus et al. 1999). The precise generation mechanisms of the low-frequency waves at the solar surface are unimportant in the context of this paper (see, e.g., Roberts 2000). The outward-propagating waves enter the corona and transform, in part, to a mixed population of outward and inward modes. Only when inward and outward wave packets are allowed to “collide” can nonlinear couplings to higher wavenumber occur. The resulting cascade is a time-steady transfer of energy from large to small spatial scales that is believed to progress by successive magnetic reconnection in the presence of the strong coronal “guide field” (e.g., Matthaeus & Lamkin 1986; Lazarian & Vishniac 1999). We assume that the turbulence becomes fully developed on time scales that are short compared to the bulk solar wind outflow and the geometrical expansion of open flux tubes. This allows us to model the turbulence as spatially homogeneous in a small volume element (with constant density and magnetic field strength) in the extended corona.

### 2.1. Definitions of Fluctuation Quantities

The energy density of fluctuations in a magnetized plasma is described most generally as a sum of electric, magnetic, and kinetic components. For linear (i.e., small amplitude) fluctuations, the total fluctuation energy density  $\delta U$  is given by

$$\delta U = \frac{\langle \delta \mathbf{E}^2 \rangle}{8\pi} + \frac{\langle \delta \mathbf{B}^2 \rangle}{8\pi} - \sum_s \int d^3 \mathbf{v} \left( \frac{1}{2} m_s |\mathbf{v}^2| \right) \frac{\langle \delta f^2 \rangle_s}{\mathbf{v} \cdot \partial f_0 / \partial \mathbf{v}} \quad (1)$$

where angle brackets denote averages over times much longer than the fluctuation time scales,  $\delta \mathbf{E}$  is the perturbed electric field, and  $\delta \mathbf{B}$  is the perturbed magnetic field (e.g., Bernstein 1958). The velocity distribution function of particle species  $s$  is assumed to be the sum of an undisturbed, stationary (zero-order) state  $f_0$  and a small, linear (first-order) perturbation  $\delta f$ . The masses and velocities of the particles are denoted  $m_s$  and  $\mathbf{v}$ , and the integration above is taken over all particle velocities for each species. For simplicity, we assume a

fully ionized plasma composed only of protons and electrons (see § 5 for a discussion of the impact of heavy ions). The quantity  $\delta U$  above is constructed as the simplest second-order and positive-definite quantity that is conserved exactly as a consequence of the fully nonlinear Vlasov equation (Davidson 1983).

If the zero-order proton and electron velocity distributions are assumed to be Maxwellian, the kinetic energy density term in eq. (1) can be expressed as the sum of fluctuations in bulk velocity and density (often referred to as “kinetic” and “thermal” energies, respectively). We assume that these two contributions to the total kinetic energy are the dominant ones, even when  $f_0$  departs from a Maxwellian form. Thus, the total energy density is given by

$$\delta U = \frac{\langle \delta \mathbf{E}^2 \rangle}{8\pi} + \frac{\langle \delta \mathbf{B}^2 \rangle}{8\pi} + \sum_s \left( \frac{1}{2} m_s n_s \langle \delta \mathbf{v}^2 \rangle_s + \frac{1}{2} k_B T_s \frac{\langle \delta n^2 \rangle_s}{n_s} \right), \quad (2)$$

where  $n_s$  and  $T_s$  are the zero-order number densities and temperatures,  $\delta \mathbf{v}$  and  $\delta n$  are the first-order velocity and number density perturbations, and  $k_B$  is Boltzmann’s constant. For a nonrelativistic plasma, the electric field term is usually negligible in comparison with the other terms. Plasmas with sufficiently strong magnetic fields tend to be dominated by incompressible magnetohydrodynamic (MHD) fluctuations (see, e.g., Goldstein, Roberts, & Matthaeus 1995), which exhibit energy density equipartition between their magnetic and proton velocity fluctuations,

$$\frac{\delta U_{\text{MHD}}}{\rho} \approx \frac{1}{2} \left( \frac{\langle \delta \mathbf{B}^2 \rangle}{4\pi\rho} + \langle \delta \mathbf{v}^2 \rangle_p \right) \approx \langle \delta \mathbf{v}^2 \rangle_p, \quad (3)$$

where  $\rho$  is the total mass density, approximately equal to its proton contribution  $m_p n_p$ . At the base of the solar corona, the total velocity amplitude  $(\delta U / \rho)^{1/2}$  is believed to be of order 20 to 40 km s<sup>−1</sup> (e.g., Mariska, Feldman, & Doschek 1978; Chae, Schühle, & Lemaire 1998). This population of waves is expected to be mostly propagating upwards from the Sun, with a radial amplitude dependence close to that predicted by the conservation of wave action (Hollweg 1973; Jacques 1977; Banerjee et al. 1998; Esser et al. 1999).

In this paper, we need to evaluate several of the terms in the total energy density  $\delta U$  independently. However, the turbulence as a whole is describable in terms

of the total fluctuation power spectrum  $W$ , defined as the energy density per unit volume in three-dimensional wavenumber space and scaled as follows

$$\frac{\delta U}{\rho} = \int d^3 \mathbf{k} W(k_{\parallel}, k_{\perp}, t). \quad (4)$$

MHD turbulence is dominated by a cascade of fluctuation energy in the direction *perpendicular* to the background magnetic field, so let us also define the reduced power spectrum quantity  $W_{\perp}$ ,

$$W_{\perp}(k_{\perp}, t) \equiv k_{\perp}^2 \int_{-\infty}^{+\infty} dk_{\parallel} W(k_{\parallel}, k_{\perp}, t), \quad (5)$$

which is proportional to the total energy density per unit  $\ln k_{\perp}$ , integrated over the parallel wavenumber  $k_{\parallel}$ . The quantity  $W_{\perp}$  has units of velocity squared, and is related to the total energy density via

$$\delta U = 2\pi\rho \int_0^{+\infty} \frac{dk_{\perp}}{k_{\perp}} W_{\perp}(k_{\perp}). \quad (6)$$

Note that  $k_{\parallel}$  can be both positive (for outward propagating waves) and negative (for inward propagating waves), but the perpendicular wavenumber  $k_{\perp}$  is positive-definite.

The energy density spectra defined above are appropriate for following the flow of the *total* energy in wavenumber space, but they do not necessarily track the dominant turbulent motions on all spatial scales. One important example is the case of large- $k_{\perp}$  kinetic Alfvén waves (KAW) that have wavelengths larger than the mean electron Larmor radius but smaller than the mean proton Larmor radius. These fluctuations are “felt” by all electrons in a similar manner as longer-wavelength MHD waves. However, some protons execute Larmor gyrations on a spatial scale larger than that of the fluctuations, and thus they become uncoupled from the waves. (Only the slowest protons—in the core of their velocity distribution—have small enough Larmor orbits to remain coupled to the electrons and waves.) Thus, even though the massive protons carry the bulk of the kinetic energy, it is the electron term  $\langle \delta \mathbf{v}^2 \rangle_e$  that most accurately describes the smallest-scale fluctuations. Let us then define  $v_{\perp}^2$  as the power spectrum of electron kinetic energy fluctuations in the perpendicular direction, which is defined in a similar manner as eq. (6),

$$\langle \delta \mathbf{v}_{\perp}^2 \rangle_e = 2\pi \int_0^{+\infty} \frac{dk_{\perp}}{k_{\perp}} v_{\perp}^2(k_{\perp}) \quad (7)$$

where only the perpendicular components of the electron velocity fluctuation are considered.<sup>1</sup> In the low- $k_\perp$  MHD limit, where protons and electrons oscillate with the same velocity,  $v_\perp^2$  is equal to  $W_\perp$ . In general, we define

$$v_\perp^2(k_\perp) = \phi_e(k_\perp) W_\perp(k_\perp) \quad (8)$$

where  $\phi_e$  describes the departure from ideal MHD energy equipartition, and is equal to 1 in the MHD limit. Formally,  $\phi_e$  is the ratio of kinetic energy density in perpendicular electron motions to the total energy density of the fluctuations at a specified wavenumber. The inverse quantity  $\phi_e^{-1}$  is also approximately equal to the number fraction of protons that remain coupled to the fluctuations at the specified wavenumber. In § 3.1 we derive the exact behavior of  $\phi_e$  as a function of  $k_\perp$ , but for simplicity we present the following approximation,

$$\phi_e \approx 1 + k_\perp^2 R_p^2, \quad (9)$$

where  $R_p$  is the mean proton gyroradius, defined as the ratio of the proton most-probable speed  $w_p = (2k_B T_p / m_p)^{1/2}$  to the proton cyclotron frequency  $\Omega_p = eB / m_p c$ . The above approximate form for  $\phi_e$  was motivated by a simple estimate of the fraction of protons that remain coupled to  $k_\perp$ -scale fluctuations; i.e.,

$$\frac{1}{\phi_e} \approx \frac{\left[ \int_0^{V_{\max}} d^2 v_\perp f_p(v_\perp) \right]}{\left[ \int_0^\infty d^2 v_\perp f_p(v_\perp) \right]}. \quad (10)$$

For a Maxwellian velocity distribution with an effective “core” defined by  $v_\perp < V_{\max} \equiv \Omega_p / k_\perp$ , the above expression yields a fraction of 1 in the limit  $k_\perp R_p \ll 1$  and a fraction of  $(k_\perp R_p)^{-2}$  in the limit  $k_\perp R_p \gg 1$ . Eq. (9) is a simple function that smoothly bridges both limits.

## 2.2. Dominant Two-Dimensional Cascade

We describe the cascade of energy in MHD turbulence as a combination of advection and diffusion in wavenumber space. Chandrasekhar (1943) developed the general statistical theory of representing stochastic processes—such as Brownian “random walks”—as

effectively diffusive. Leith (1967) proposed a general advection-diffusion equation for the evolution of fluctuation power in isotropic hydrodynamic turbulence. Leith’s chief assumption was that the spectral cascade term must only redistribute energy in wavenumber space and should not alter its total magnitude. Thus, the spectral cascade term was written as the divergence of a flux-like quantity, where the primary contribution to the flux is from nearby regions of wavenumber space (e.g., Kolmogorov 1941; Obukhov 1941). Pao (1965), Eichler (1979), Tu, Pu, & Wei (1984), and Tu (1988) modeled the spectral transfer as pure advection by deriving dimensionally consistent flux quantities that are scalar functions of the local wave power and wavenumber. Zhou & Matthaeus (1990) applied Leith’s (1967) cascade phenomenology to MHD turbulence and derived diffusion coefficients consistent with both the Kolmogorov (1941) and Kraichnan (1965) energy transfer rates.

It has been known for several decades that MHD turbulence in the presence of a background magnetic field develops a strong wavenumber anisotropy. Both numerical simulations and analytic descriptions such as “reduced MHD” (RMHD) have indicated that cascade from large to small spatial scales proceeds mainly in the two-dimensional plane perpendicular to the background field  $\mathbf{B}_0$  (e.g., Strauss 1976; Montgomery 1982; Shebalin, Matthaeus, & Montgomery 1983; Matthaeus et al. 1996; Goldreich & Sridhar 1995, 1997; Maron & Goldreich 2001; Bhattacharjee & Ng 2001; Cho, Lazarian, & Vishniac 2002). We apply the Zhou & Matthaeus (1990) wavenumber diffusion idea to this largely two-dimensional transfer of energy from small  $k_\perp$  to large  $k_\perp$ .

We model the interplay of wave injection (at small  $k_\perp$ ), cascade, and damping (at large  $k_\perp$ ) with an advection-diffusion equation similar to those used by Zhou & Matthaeus (1990), Miller, LaRosa, & Moore (1996), and Stawicki, Gary, & Li (2001). The  $k_\parallel$ -integrated fluctuation power is assumed to obey the following transport equation,

$$\frac{\partial W_\perp}{\partial t} = \frac{\partial}{\partial x} \left[ \frac{1}{\tau_s} \left( -\beta W_\perp + \gamma \frac{\partial W_\perp}{\partial x} \right) \right]$$

---

<sup>1</sup>For kinetic Alfvén waves, the parallel electron velocity fluctuation begins to dominate when  $k_\perp$  becomes of the same order as the inverse ion inertial length (see Hollweg 1999a). However, we restrict the definition of  $v_\perp$  to the perpendicular fluctuations in order to be consistent with anisotropic MHD turbulence theory.

$$+ S(k_{\perp}) - D(k_{\perp})W_{\perp} \quad , \quad (11)$$

where  $x = \ln k_{\perp}$ ,  $\tau_s$  is a characteristic spectral transfer time, and  $\beta$  and  $\gamma$  are dimensionless constants. The  $S$  term describes the source of energy at low  $k_{\perp}$ , which presumably propagates up from the Sun in the form of low-frequency Alfvén waves. The  $D$  term describes the dissipation of energy at high  $k_{\perp}$ . The local spectral transfer time  $\tau_s$  is assumed to be equal to the nonlinear time scale  $(k_{\perp}v_{\perp})^{-1}$  (Batchelor 1953; Goldreich & Sridhar 1995). We use the perpendicular electron spectrum  $v_{\perp}(k_{\perp})$  to track the turbulent motions on all scales, which introduces a factor of  $\phi_e^{1/2}$  into the advection-diffusion equation when  $\tau_s$  is written in terms of  $W_{\perp}$ .

Note that we did not include in eq. (11) any large-scale transport terms that depend on radial gradients of the coronal plasma parameters. This is in accord with the assumption discussed above that the cascade acts on a time scale that is short in comparison to representative flow times (due to wind advection, wave propagation, or geometrical expansion) over a coronal scale height. The interaction between large-scale “sweeping” terms in the corona and local turbulent cascade effects is discussed in detail by Leamon et al. (2000).

The nonlinear cascade process modeled in eq. (11) reflects some of the physics of wave dispersion and damping, but not all. The spectral transfer time  $\tau_s$  behaves differently in the ideal MHD regime ( $\phi_e \approx 1$ ) and in the KAW regime ( $\phi_e \propto k_{\perp}^2$ ). Moreover, the dissipation term  $D$  in these regimes behaves as a power-law in  $k_{\perp}$ , thus producing a phenomenology very similar to that of viscosity in fluid turbulence (e.g., Pao 1965; Leith 1967). However, we do not include high-frequency (proton cyclotron) dispersive effects in the cascade term, even though we do include them in the dissipation term.<sup>2</sup> Such effects in the cascade term are expected to be negligible because of the very limited extent of the “dispersion range” in  $k_{\parallel}$  (see the closely-spaced solid contours in Figure 4a, below). Therefore, cyclotron dispersion cannot substantially affect the rate of energy transport from low to high  $k_{\parallel}$ . In future work we intend to explore more self-consistent cascade phenomenologies for plasmas of arbitrary  $k_{\parallel}$  and  $k_{\perp}$ .

In order to specify the  $\beta$  and  $\gamma$  constants as independent advection and diffusion strengths, we follow the statistical analysis of van Ballegoijen (1986). In the “random walk” limit that individual turbulent displacements are small compared to the outer-scale correlation length, van Ballegoijen (1986) found that  $\beta \approx \gamma$ . We assume for simplicity that  $\beta$  and  $\gamma$  are constants (i.e., independent of wavenumber). We also assume that  $\beta$  and  $\gamma$  are of order unity because the primary physics of the cascade is encapsulated in the spectral transfer time  $\tau_s$ . Our baseline model thus assigns  $\beta = \gamma = 1$ , and other models vary either  $\beta$  or  $\gamma$  while keeping the other equal to 1. The most appropriate values of these constants to use in the extended solar corona should be determined ultimately from the analysis of numerical simulations or laboratory experiments.

Figure 1 shows representative time-steady solutions to eq. (11) computed using a Crank-Nicholson numerical finite differencing scheme. The Appendix contains further details about the solution method and the definition of supplementary quantities. The low-wavenumber source term  $S(k_{\perp})$  was defined as a narrow Gaussian function that injects most of its energy at an outer-scale length  $L_{\text{out}} \sim k_{\text{out}}^{-1}$  that we specified as approximately 3800 km. This value is consistent with the photospheric granulation scale (1000 km) expanded superradially in a polar coronal hole out to a distance of  $2 R_{\odot}$  (i.e.,  $L_{\text{out}} \propto B_0^{-1/2}$ ; see Hollweg 1986). The coronal hole magnetic field structure is assumed to follow the dipole/quadrupole/current-sheet model of Banaszkiewicz, Axford, & McKenzie (1998). Note also that a similar outer-scale length ( $\sim 1200$  km at the base) was derived—independently of granulation observations—by Chae et al. (1998), who balanced an empirical turbulent heating rate by local radiative losses in the transition region and low corona. We assume that the wave energy at the outer scale is generated at the solar surface, propagates outward into the corona, and undergoes some degree of transformation into a mixed population of outward and inward modes (by, e.g., reflection). The dissipation term  $D(k_{\perp})$  used in the models shown in

---

<sup>2</sup>One can avoid possible inconsistencies of this kind by assuming the wavelength ranges of cascade and dissipation are separated from one another. However, this allows only the computation of the total energy fluxes and not a detailed comparison of relative proton/electron and parallel/perpendicular heating rates; see also Leamon et al. (1999, 2000).

Figure 1 was assumed to be similar to that of standard kinematic viscosity; i.e.,  $D \propto k_{\perp}^2$ . We plot the power spectra computed with three different normalizing constants for the dissipation term.

The solutions for  $W_{\perp}(k_{\perp})$  fall into several regimes of wavenumber. For  $k_{\perp} \ll k_{\text{out}}$ , there is no significant turbulent cascade, and the residual power decays like  $W_{\perp} \propto k_{\perp}^{\beta/\gamma}$  as a result of the ever-present diffusion. The power spectrum peaks around  $k_{\text{out}}$  at a maximum value that depends on the integrated total energy. In Figure 1, we specify  $(\delta U/\rho)^{1/2} = 50 \text{ km s}^{-1}$ , which results in a maximum value of  $W_{\perp}^{1/2}$  of about  $10.2 \text{ km s}^{-1}$ . The factor-of-5 difference between these two quantities is a simple consequence of the shape of  $W_{\perp}(k_{\perp})$  around the peak at  $k_{\text{out}}$ . For  $k_{\perp} > k_{\text{out}}$ , the power spectrum begins to decrease in an MHD power-law inertial range, with a Kolmogorov-Obukhov spectral index  $W_{\perp} \propto k_{\perp}^{-2/3}$  (the standard one-dimensional power spectrum is given by  $W_{\perp}/k_{\perp} \propto k_{\perp}^{-5/3}$ ; see eq. [6] and the detailed derivation in the Appendix). The spectral index in the inertial range does not depend on  $\beta$  or  $\gamma$ , but only on the wavenumber and power dependence of  $\tau_s$ . As  $k_{\perp}$  approaches the inverse proton gyroradius, however, the factor  $\phi_e$  in  $\tau_s$  becomes larger than 1, and the inertial range spectral index steepens from  $-2/3$  to  $-4/3$ . We refer to these wavenumber regions below as the MHD and KAW inertial ranges, respectively (see also discussion of the “dispersion range” in interplanetary space by Stawicki et al. 2001). At high  $k_{\perp}$ , where  $D$  becomes of the same order as the local cascade rate  $\tau_s^{-1}$ , the power spectrum dissipates rapidly.

### 2.3. Extension into Parallel Wavenumber

The previous section described the dynamics of turbulence as a function of  $k_{\perp}$  and ignored the behavior of the full power spectrum  $W$  as a function of  $k_{\parallel}$ . The strong predicted anisotropy of MHD turbulence justifies this approach to first order, but we are also concerned with the possible “leakage” of power to high values of  $k_{\parallel}$  and thus to high frequencies. A substantial amount of power at the cyclotron frequencies of positive ions would lead to significant preferential ion heating.

Let us model the spectral transport in  $k_{\parallel}$  with a diffusion term similar to that assumed above. It should be

emphasized, however, that the actual parallel transport is probably *nonlocal* in wavenumber space (due to, e.g., intermittent high-order wave-wave interactions and nonlinear steepening; see Medvedev 2000) and thus should not be describable by local diffusion. Our primary goal is to recover the phenomenology of the anisotropic “critical balance” described by Goldreich & Sridhar (1995) and not to model the physics of nonlocal turbulent transport in detail. We thus propose the following advection-diffusion equation for  $W(\mathbf{k})$ :

$$\frac{\partial W}{\partial t} = \frac{1}{k_{\perp}} \frac{\partial}{\partial k_{\perp}} \left\{ k_{\perp} v_{\perp} \left[ -\beta k_{\perp}^2 W + \gamma k_{\perp} \frac{\partial}{\partial k_{\perp}} (k_{\perp}^2 W) \right] \right\} + \alpha k_{\perp} v_{\perp} \tilde{k}_{\parallel}^2 \left( \frac{\partial^2 W}{\partial k_{\parallel}^2} \right) + S' - DW \quad (12)$$

which has been written in this way in order to recover eq. (11) when each term above is multiplied by  $k_{\perp}^2$  and integrated over  $k_{\parallel}$ . The dimensionless parameter  $\alpha$ , presumably of the same order as  $\beta$  and  $\gamma$ , determines the relative strength of the effective parallel cascade. The wavenumber scale is set by  $\tilde{k}_{\parallel}$ , which is a typical parallel wavenumber determined from the condition of critical balance (i.e., strong coupling between turbulent mixing motions and Alfvén-wave motions along the field). Let us define the dimensionless ratio

$$y \equiv \frac{\omega_r}{k_{\perp} v_{\perp}} = k_{\parallel} / \tilde{k}_{\parallel} \quad (13)$$

where  $\omega_r$  is the real frequency of Alfvén waves as a function of  $k_{\parallel}$  and  $k_{\perp}$ , and the Goldreich-Sridhar condition of critical balance is equivalent to the condition  $y = 1$ . The source term  $S'(\mathbf{k})$  in eq. (12) is related to the source term in eq. (11) as follows,

$$S(k_{\perp}) = k_{\perp}^2 \int_{-\infty}^{+\infty} dk_{\parallel} S'(k_{\parallel}, k_{\perp}) , \quad (14)$$

and we assume  $D(\mathbf{k})$  is dominated by the same kinetic sources of damping that were assumed in § 2.2.

The advection-diffusion equation presented above does not depend on the sign of  $k_{\parallel}$ , and thus it produces diffusion for waves propagating in both directions along the magnetic field. In this paper we assume that  $W$  is symmetric about  $k_{\parallel} = 0$  (i.e., that the net cross helicity of the fluctuations is zero). This is consistent with the analysis of Goldreich & Sridhar (1995), but is manifestly not true for the lowest- $k_{\perp}$  (energy-containing) modes at

the outer scale in the corona. For these large-scale waves, there should be more power on the outward-propagating side ( $k_{\parallel} > 0$ ) than on the inward-propagating side. However, as the cascade proceeds to higher wavenumbers, the power in outward and inward propagating modes should become increasingly mixed (see, e.g., Roberts et al. 1992; Vasquez, Markovskii, & Hollweg 2002). The main reason we are modeling  $W(\mathbf{k})$  in this paper is to compute the kinetic dissipation and particle heating *at high wavenumber*, so the assumption that the outward and inward power is equal seems justifiable.

In order to evaluate the quantity  $y$  defined above, we estimate the dispersion relation for kinetic Alfvén waves (KAW) as  $\omega_r \approx k_{\parallel} V_A \phi_e^{1/2}$ . This relation assumes frequencies much lower than the proton cyclotron frequency (see § 3.1 for a more complete discussion of dispersion). The multiplicative factor of  $\phi_e^{1/2}$  represents the lower inertia in the KAW regime due to the decoupling of protons from the wave motions. The coupled-proton fraction  $1/\phi_e$  can be considered to be proportional to the effective “mass”  $m$  of a body undergoing simple harmonic motion; the frequency of oscillations for such a body scales as  $\omega^2 \sim \kappa/m$ , where  $\kappa$  is the effective “spring constant” determined here by the Alfvén speed  $V_A$ . Because both the numerator and denominator in eq. (13) contain factors of  $\phi_e^{1/2}$ , the quantity  $y$  can be expressed as

$$y \approx \frac{k_{\parallel} V_A}{k_{\perp} W_{\perp}^{1/2}}, \quad (15)$$

which is essentially the inverse of the Goldreich & Sridhar (1995) nonlinearity parameter  $\zeta$ . We use this approximation to derive an analytic solution for  $W(k_{\parallel}, k_{\perp})$ , but in § 3.2 we replace the above relation with the complete definition for  $y$  (eq. [13]) and use a numerical solution for  $\omega_r$ .

In the MHD inertial range,  $W_{\perp}$  is proportional to  $k_{\perp}^{-2/3}$ , and thus  $y \propto k_{\parallel} k_{\perp}^{-2/3}$ . Turbulent eddies that conform to the condition of critical balance ( $y = 1$ ) exhibit a wavenumber scaling of  $k_{\parallel} \propto k_{\perp}^{2/3}$ , which implies they become increasingly elongated in the direction of the magnetic field as the cascade proceeds to higher wavenumber. This spectral anisotropy is discussed in more detail by, e.g., Goldreich & Sridhar (1995), Maron & Goldreich (2001), and Cho et al. (2002), and possible observational evidence of such elongated inhomogeneities was presented by Grall et al. (1997). In the

KAW inertial range, the elongation should grow slightly stronger, with  $y \propto k_{\parallel} k_{\perp}^{-1/3}$ . However, dissipation is believed to set in around  $k_{\perp} R_p \sim 1$ , before too much of the KAW inertial range can develop.

To solve eq. (12) we make the important assumption that  $W$  is a separable function of two variables:  $k_{\perp}$  and  $y$ . Following Goldreich & Sridhar (1995), we write the wave power spectrum as

$$W(k_{\perp}, y) = \frac{V_A W_{\perp}^{1/2}}{k_{\perp}^3} g(y) \quad (16)$$

which was defined in this way to ensure that the dimensionless function  $g(y)$  is normalized to unity,

$$\int_{-\infty}^{+\infty} dy g(y) = 1, \quad (17)$$

and also that eqs. (4)–(6) are satisfied. The solution for  $W_{\perp}(k_{\perp})$  is discussed above in § 2.2, and the Appendix shows how a known solution for  $W_{\perp}$  allows eq. (12) to be approximated as an ordinary differential equation for  $g(y)$ . The solution to this differential equation in the inertial range is

$$g(y) \propto \left[ 1 + \frac{\gamma(1 - \zeta)^2 y^2}{\alpha} \right]^{-n} \quad (18)$$

with the normalization determined by eq. (17), and

$$n = \frac{(\beta/\gamma) + \zeta + 1}{2(1 - \zeta)} \quad (19)$$

(see Appendix for details). The dimensionless exponent  $\zeta$  is defined by

$$2\zeta = -\frac{k_{\perp}}{W_{\perp}} \frac{\partial W_{\perp}}{\partial k_{\perp}}, \quad (20)$$

and in the MHD and KAW inertial ranges,  $\zeta = 1/3$  and  $2/3$ , respectively. The above solution for  $g(y)$  superficially resembles a generalized Lorentzian, or kappa distribution (Olbert 1969), which is Gaussian for small arguments and approaches a power-law tail for large arguments. Cho et al. (2002) analyzed numerical turbulence simulations and found that  $g(y)$  may be fit reasonably well by decaying exponential or Castaing functions. However, the simulations do not seem to have sufficient dynamic range in the high- $k_{\parallel}$  modes to resolve a possible power-law tail as in eq. (18).

The relative amount of wave dissipation that heats protons and heavy ions depends sensitively on the power that diffuses to high frequencies; i.e.,  $y \gg 1$ . In this limit, the above analytic solution in the inertial range behaves as  $g \propto y^{-2n}$ , which (after normalization) no longer depends on the parallel diffusion coefficient  $\alpha$ . Thus, even when  $y \gg 1$ , the dominant diffusion still comes from the perpendicular  $\beta$  and  $\gamma$  terms. The major contribution of the  $\alpha$  term is to “bootstrap” the transport of power from low to high  $k_{\parallel}$ ; the perpendicular transport then takes over to determine the residual  $k_{\parallel}$ -dependence of the power spectrum. A key parameter in the  $y$ -dependence of the power-law tail is the ratio  $\beta/\gamma$ , which is the relative strength of perpendicular advection over that of diffusion. We extend our baseline assumption of the previous section and assume  $\alpha = \beta = \gamma = 1$ , but for cases when the ratio  $\beta/\gamma$  is varied we keep the two *diffusion* coefficients equal to one another ( $\alpha = \gamma$ ).

### 3. Wave Dispersion and Dissipation

#### 3.1. Vlasov-Maxwell Kinetic Theory

Once the total fluctuation power spectrum  $W(\mathbf{k})$  is known, it becomes possible to compute the relevant particle heating rates in the extended corona. Despite the fact that the strong, critically balanced turbulence described above is not very “wavelike” (i.e., a coherent wave survives for only about one period before nonlinear processes transfer its energy to smaller scales), we follow the standard procedure of using the linear wave dispersion relation to compute frequencies and dissipation rates (see also Miller et al. 1996; Quataert 1998; Leamon et al. 1999). The amplitudes of the waves in the dissipation range are extremely small (i.e.,  $\langle \delta B^2 \rangle \ll B_0^2$ ), so the assumption of linearity is probably adequate. In at least one other turbulent astrophysical plasma—the interstellar medium—a comprehensive study of various dissipation mechanisms (Spangler 1991) showed that linear damping processes are most likely to be stronger than nonlinear damping processes.

We solve the linear dispersion relation for the real and imaginary parts of the frequency in the solar-wind frame ( $\omega = \omega_r + i\omega_i$ ) assuming a known real wavevector  $\mathbf{k}$ . The

Vlasov-Maxwell dispersion relation,

$$\frac{c^2}{\omega^2} [\mathbf{k} \times (\mathbf{k} \times \mathbf{E})] + \tilde{\epsilon} \cdot \mathbf{E} = 0 \quad , \quad (21)$$

is derived by linearizing and Fourier transforming Maxwell’s equations (see, e.g., Stix 1992; Krauss-Varban, Omid, & Quest 1994; Brambilla 1998). Above,  $\mathbf{E}$  is the perturbed electric field,  $c$  is the speed of light, and  $\tilde{\epsilon}$  is the dielectric tensor constrained by the linearized Vlasov equation. The dispersion relation is essentially a  $3 \times 3$  matrix multiplying  $\mathbf{E}$ , and we solve for the complex values of  $\omega$  that make the determinant of this matrix zero. We use the numerical Newton-Raphson technique to isolate individual solutions from a grid of starting guesses in  $\omega_r, \omega_i$  space. Besides the assumption of Maxwellian distributions (see below) and the use of numerical expansions for Bessel functions and the plasma dispersion function (Fried & Conte 1961; Poppe & Wijers 1990), the kinetic dispersion tensor is calculated exactly. The nine elements of  $\tilde{\epsilon}$  at each solution allow us to compute the electric field polarization vectors and the relative amounts of wave energy in electric, magnetic, kinetic, and thermal perturbations for each wave mode (see eq. [2] and Appendix 1 of Krauss-Varban et al. 1994).

We model the local plasma conditions at a heliocentric distance of  $2 R_{\odot}$  in the accelerating high-speed solar wind. The magnetic field is given by the polar coronal-hole flux tube model of Banaszekiewicz et al. (1998), with  $\Omega_p = 7660 \text{ rad s}^{-1}$ . The coronal-hole electron density  $n_e$  at  $2 R_{\odot}$  has been constrained to be between  $2 \times 10^5$  and  $7 \times 10^5 \text{ cm}^{-3}$ , depending on the relative concentration of polar plumes (Cranmer et al. 1999b). We choose a value within this range that sets the Alfvén speed  $V_A$  to be exactly  $2000 \text{ km s}^{-1}$ . For the purpose of computing the wave dispersion, we assume isotropic Maxwellian distributions for the protons and electrons with temperatures constrained empirically as follows:  $T_e = 8 \times 10^5 \text{ K}$ ,  $T_p = 2 \times 10^6 \text{ K}$  (Kohl et al. 1997, 1998; Esser et al. 1999; Doschek et al. 2001). The plasma beta, here denoted as  $\tilde{\beta}$  to distinguish it from the cascade advection strength  $\beta$ , is defined as the ratio of the total plasma pressure to the magnetic pressure,

$$\tilde{\beta} \equiv \frac{8\pi}{B_0^2} \sum_s n_s k_B T_s \approx 0.009 \quad , \quad (22)$$

where the numerical value pertains to the coronal conditions described above. At all heights in the corona,

$\tilde{\beta} \ll 1$ , but this quantity always remains larger than the electron-to-proton mass ratio  $m_e/m_p$ .

In this paper we concentrate only on the solution branch corresponding to shear Alfvén waves. This mode is expected to be dominant in the limit of nearly incompressible MHD turbulence (Goldstein et al. 1995; Tu & Marsch 1995), and here we follow the evolution of Alfvénic fluctuations both to the high-frequency ion cyclotron limit and to the high- $k_\perp$  KAW limit. The Alfvén mode is identified clearly at the lowest wavenumbers in our computational grid ( $k_\parallel V_A/\Omega_p = 10^{-7}$  and  $k_\perp R_p = 10^{-6}$ ), and it is tracked incrementally as either  $k_\parallel$  or  $k_\perp$  is increased slowly. We ignore the fast and slow magnetosonic wave modes—and thus possibly underestimate the full heating rates in the extended corona—but these types of waves have long been thought to be damped substantially before they can reach the corona. We also ignore high-frequency plasma waves such as Langmuir and hybrid modes (which are expected to be much smaller in amplitude than the lower-frequency MHD waves) as well as other strongly damped solutions with no fluid counterparts (such as the Bernstein modes).

Figures 2 and 3 show example solutions of the dispersion relation for various ranges of wavenumber. Figure 2a plots the real and imaginary parts of the frequency for a constant value of  $k_\parallel$  (in the low-frequency limit,  $\omega_r \ll \Omega_p$ ) as a function of  $k_\perp$ . This figure thus illustrates the evolution of the KAW in the limit of large obliqueness angles. The ratio  $|\omega_i/\omega_r|$  is negligibly small for small values of  $k_\perp$ , but it grows to a value of order 0.2 in the KAW limit ( $k_\perp R_p \gtrsim 1$ ). The damping for all plotted values of  $k_\perp$  is dominated by the linear Landau resonance. Figure 2b plots the relative contributions to the total linearized energy density of the waves as defined in eq. (2). In the low- $k_\perp$  MHD limit, there is equipartition between the magnetic field term and the proton kinetic term (i.e., transverse velocity oscillations). When there is significant KAW dispersion, though, the electron kinetic term becomes important as fewer protons remain coupled to the small-scale fluctuations. “Thermal” density fluctuations also become non-negligible (Hollweg 1999a). The protons and electrons exhibit identical relative density oscillations  $\delta n/n$ , but the proton thermal energy density is larger because  $T_p = 2.5T_e$ . The quantity  $\phi_e$  (eq. [8]), which is defined as the ratio of kinetic energy in perpendicular electron fluctuations to the total

energy density, is also plotted in Figure 2a.

In the low-frequency, highly oblique KAW limit, the Alfvén branch ceases to exist for perpendicular wavenumbers greater than  $k_\perp R_p \approx 14$ . This occurs when the parallel phase speed of the waves  $\omega_r/k_\parallel$  exceeds approximately two times the electron most-probable speed, and the number of electrons available to participate in coherent wave motions (in the tail of the distribution) becomes increasingly small. We believe this also explains the departure from the simple analytic KAW dispersion relation,

$$\omega_r \approx k_\parallel V_A \sqrt{1 + k_\perp^2 R_p^2}, \quad (23)$$

where a temperature-dependent, order-unity factor multiplying the  $k_\perp^2$  term has been omitted. The above expression assumes full coupling between the waves and the entire velocity distribution. The cessation of solutions occurs at higher perpendicular wavenumbers for higher  $\tilde{\beta}$  plasmas.

For higher wavenumbers ( $k_\perp R_p \gtrsim 14$ ) in the low- $\tilde{\beta}$  plasma considered here, the kinetic extension of the fast-mode magnetosonic wave is the only surviving solution with similar dispersion properties as the KAW. This mode is similarly longitudinal (i.e., with its electric field polarization vector nearly parallel to its wavevector), and it exhibits a similar distribution of energy density fractions as in the rightmost part of Figure 2b. Although we expect the turbulent cascade to deposit some power into this new mode once the KAW solutions disappear, we neglect this mode henceforth in order to determine how much of the turbulent energy is absorbed by the purely Alfvénic fluctuations.

Figure 3 displays the dispersion properties of nearly parallel-propagating Alfvén waves versus  $k_\parallel$  (with  $k_\perp R_p$  held constant at  $10^{-3}$ ) as the wave frequency approaches the proton cyclotron frequency. The numerically computed frequency comes close to that of the cold-plasma approximation,

$$\omega_r \approx k_\parallel V_A \sqrt{1 - \frac{\omega_r}{\Omega_p}} \quad (24)$$

(e.g., Dusenbery & Hollweg 1981). The damping rate  $\omega_i$  contains two contributions: one due to Landau damping (at low  $k_\parallel$ ) and one due to the proton cyclotron resonance (at high  $k_\parallel$ ). The waves in this regime are nearly incompressible, with the magnetic energy density varying from

equipartition with proton bulk motions in the MHD limit, to near dominance of the total fluctuation energy in the limit  $\omega_r \rightarrow \Omega_p$  (see Figure 3b).

We find that the Alfvénic proton cyclotron branch ceases to exist for parallel wavenumbers greater than  $k_{\parallel} V_A / \Omega_p \approx 3.4$ . This “warm plasma” effect was predicted to occur by Stix (1992) at about

$$\frac{k_{\parallel \max} V_A}{\Omega_p} = \pi^{1/6} \left( \frac{V_A}{w_{\parallel p}} \right)^{1/3}, \quad (25)$$

where  $w_{\parallel p}$  is the parallel proton most-probable speed, and this quantity is  $\sim 2.7$  in the plasma conditions modeled here. The 20% difference between the predicted and actual cutoff values probably occurs because of the different assumed proton and electron temperatures (electron contributions are ignored in the above expression).

We computed the real and imaginary parts of the Alfvén-mode frequency  $\omega$  in a grid that extended from  $10^{-7}$  to 3.4 (in  $k_{\parallel} V_A / \Omega_p$ ) and from  $10^{-6}$  to 14.2 (in  $k_{\perp} R_p$ ). Specifically,  $\omega_i$  is the growth or damping rate (growth if positive; damping if negative) for the electric field perturbation amplitude. In order to determine the positive-definite damping rate for the dominant two-dimensional cascade of energy (proportional to the square of the amplitude), we set the quantity  $D$  in eq. (11) equal to  $-2\omega_i$ . We selected a locus of points in the wavenumber grid that traces out the critical balance condition of  $y = 1$ , with  $y$  defined preliminarily by the *undamped* spectrum  $W_{\perp}$ . For most values of the wave power that we considered, the  $y = 1$  curve occurs where the wavevectors are extremely oblique ( $k_{\perp} \gg k_{\parallel}$ ), and thus they are in the KAW regime plotted in Figure 2. For these low-frequency fluctuations, the ratio  $\omega_i / \omega_r$  depends only on  $k_{\perp}$ , and we can write the frequency and the critically balanced damping rate along the  $y = 1$  curve as

$$\omega_r = k_{\perp} v_{\perp} = k_{\perp} \phi_e^{1/2} W_{\perp}^{1/2},$$

$$D(k_{\perp}) = -2\omega_i = -\frac{2\omega_i}{\omega_r} k_{\perp} \phi_e^{1/2} W_{\perp}^{1/2}. \quad (26)$$

We found a parameterized fit for the  $k_{\perp}$  dependence of the ratio  $\omega_i / \omega_r$  and combined it with eq. (9) to derive the following expression for the damping rate along the

$y = 1$  curve:

$$D(k_{\perp}) \approx (5.95 \times 10^{-5} \text{ cm}^{-1}) \frac{k_{\perp}^3 R_p^3 W_{\perp}^{1/2}}{(1 + 0.7 k_{\perp}^2 R_p^2)^{1/2}}. \quad (27)$$

The numerical factor on the right-hand side applies specifically to the adopted coronal conditions at  $2 R_{\odot}$ . Also, this parameterization is valid only for the range of wavenumber where there are Alfvénic solutions (i.e.,  $k_{\perp} R_p \lesssim 14$ ). In the MHD limit, where  $k_{\perp} R_p \ll 1$ ,  $D(k_{\perp})$  is proportional to  $k_{\perp}^{8/3}$ , which is close to—but slightly steeper than—the commonly assumed viscous damping relation  $D \propto k_{\perp}^2$ .

### 3.2. Quasi-linear Proton and Electron Heating

The above calculation of the damping rate  $\omega_i$  does not reveal the relative amounts of energy absorbed by protons or electrons, nor does it describe how the particle velocity distributions are driven away from isotropy. In this section we compute individual proton and electron heating rates (in both the parallel and perpendicular directions) and bulk acceleration rates, based on assumptions utilized by Quataert (1998), Quataert & Gruzinov (1999), and Marsch & Tu (2001). The individual heating and acceleration rates are computable in closed form in the quasi-linear limit (i.e., if  $|\omega_i| \ll \omega_r$ ). We use this assumption to compute only the relative fractions of energy in the various rates, and normalize the total energy dissipation by the numerically computed (not quasi-linear) values of  $\omega_i$  from the previous section.

The approach used in this paper differs from that of Leamon et al. (1999), who isolated the electron and proton contributions to the turbulent heating rate by comparing their baseline calculation with a trial calculation with an extremely low electron  $\tilde{\beta}$ . The approach of Leamon et al. retained the full solution of the linear dispersion relation (even for  $|\omega_i| \approx \omega_r$ ), but at the expense of having to assume an unrealistically small electron temperature. Leamon et al. (1999) also evaluated the KAW dispersion relation in plasma conditions appropriate for the *in situ* solar wind ( $r \gtrsim 20 R_{\odot}$ ), whereas we are concerned with the corona.

To retain the greatest generality, we assume a bi-

Maxwellian velocity distribution for each species  $s$ ,

$$f_{0,s}(v_{\parallel}, v_{\perp}) = \frac{n_s}{\pi^{3/2} w_{\parallel s} w_{\perp s}^2} \times \exp \left[ - \left( \frac{v_{\parallel} - u_{\parallel s}}{w_{\parallel s}} \right)^2 - \frac{v_{\perp}^2}{w_{\perp s}^2} \right], \quad (28)$$

where  $u_{\parallel s}$  is the bulk speed along the magnetic field and  $w_{\parallel s}$  and  $w_{\perp s}$  are the anisotropic most-probable speeds. These quantities relate to the temperatures via

$$w_{\parallel s}^2 \equiv 2k_{\text{B}}T_{\parallel s}/m_s, \quad w_{\perp s}^2 \equiv 2k_{\text{B}}T_{\perp s}/m_s. \quad (29)$$

Let us define the damping rate that is attributable to particle species  $s$  as a positive quantity:

$$\omega_{i,s} \equiv -\omega_i \left\{ \frac{\omega_{ps}^2 (\omega_r - u_{\parallel s} k_{\parallel}) K_s^{(0)}}{\sum_t \omega_{pt}^2 (\omega_r - u_{\parallel t} k_{\parallel}) K_t^{(0)}} \right\} \quad (30)$$

where  $\omega_{ps} = (4\pi q_s^2 n_s / m_s)^{1/2}$  is the plasma frequency of species  $s$  and  $q_s$  is the charge on particle  $s$ . The denominator of eq. (30) ensures that the sum of  $\omega_{i,s}$  over all species must be equal to the magnitude of  $\omega_i$ . We define the generalized resonance function  $K_s^{(m)}$  as

$$K_s^{(m)} \equiv \sum_{\ell=-\infty}^{+\infty} \ell^m \mathcal{R}_s(\mathbf{k}, \ell) \quad (31)$$

where  $\mathcal{R}_s(\mathbf{k}, \ell)$  is the linear Landau/cyclotron resonance function given by eqs. (42)–(45) of Marsch & Tu (2001) and  $m$  is an integer. The quantity  $\mathcal{R}_s$  depends on complicated functions of  $\omega$ ,  $\mathbf{k}$ , and the electric field polarization vector, and is too lengthy to reproduce here. Linear wave-particle resonances are included in this quantity as factors of the form

$$\exp \left[ - \left( \frac{\omega - u_{\parallel s} k_{\parallel} - \ell \Omega_s}{w_{\parallel s} k_{\parallel}} \right)^2 \right] \quad (32)$$

where  $\ell = 0$  corresponds to Landau damping and transit time magnetic pumping (the latter believed to be important only when  $\tilde{\beta} \gtrsim 1$ ), and  $\ell \neq 0$  corresponds to cyclotron or gyroresonant damping. In the models presented below, we compute  $\mathcal{R}_s$  fully for the Alfvén modes discussed in the previous section, and we sum  $K_s^{(m)}$  over  $\ell$  from  $-20$  to  $+20$ . Test runs with larger ranges of  $\ell$  have ensured that no quantitative results depended on this choice of lower and upper summation bounds.

Marsch & Tu (2001), following Melrose (1986) and others, wrote the particle heating rates as an integration over either a magnetic or an electric power spectrum. We have rewritten these rates in terms of  $W(\mathbf{k})$  and  $\omega_{i,s}$  by noting that the total heating rate for species  $s$  ( $Q_s$ ) should be balanced by the damping of the total fluctuation spectrum, i.e.,

$$Q_s = Q_{\parallel s} + Q_{\perp s} = n_s k_{\text{B}} \frac{\partial}{\partial t} \left( \frac{T_{\parallel s}}{2} + T_{\perp s} \right) = \rho \int d^3 \mathbf{k} W(\mathbf{k}) 2\omega_{i,s}. \quad (33)$$

The individual resonant acceleration and heating rates are thus given by an analogue of eqs. (27) and (33) of Marsch & Tu (2001):

$$m_s n_s \frac{\partial}{\partial t} \left\{ \begin{array}{c} u_{\parallel s} \\ w_{\parallel s}^2 \\ w_{\perp s}^2 \end{array} \right\} \equiv \left\{ \begin{array}{c} A_{\parallel s} \\ 4Q_{\parallel s} \\ 2Q_{\perp s} \end{array} \right\} = \rho \int d^3 \mathbf{k} W(\mathbf{k}) \left( \frac{2\omega_{i,s}}{\omega_r - u_{\parallel s} k_{\parallel}} \right) \times \left\{ \begin{array}{c} k_{\parallel} \\ 4(\omega_r - u_{\parallel s} k_{\parallel}) - 4\Omega_s K_s^{(1)}/K_s^{(0)} \\ 2\Omega_s K_s^{(1)}/K_s^{(0)} \end{array} \right\}. \quad (34)$$

For consistency with the assumptions in § 3.1, we have solved the above equations for isotropic Maxwellians ( $w_{\parallel s} = w_{\perp s}$ ) and in the frame of the solar wind's bulk outflow (i.e.,  $u_{\parallel s} = 0$ ). The resonant acceleration term presented above is given only for completeness. It has been shown that  $A_{\parallel s}$  is probably not an important contributor to solar wind acceleration, since the magnetic mirror force is typically stronger by a wide margin (e.g., Hollweg 1999b, Cranmer 2001).

To evaluate eq. (34), the wave spectrum  $W(k_{\parallel}, k_{\perp})$  must be specified on the same grid of wavenumber points as in the dispersion calculation. The two-dimensional wave spectrum  $W_{\perp}(k_{\perp})$  was first computed with no damping in order to specify the location of the  $y = 1$  curve, then it was recomputed with the damping rate  $D(k_{\perp})$  given in eq. (27). The change in  $W_{\perp}$  did not significantly affect the position of the  $y = 1$  curve in wavenumber space, so further iteration was not needed. We used the full numerical solutions for  $\omega_r$  and  $\phi_e$  in the definition of  $y$  so that many of the simplifying assumptions in § 2.3 did not need to be applied. However, the analytic expression for  $g(y)$  in eqs. (18) and (19) was

used, with  $\zeta$  given by a simple undamped approximation that applies in the MHD and KAW limits,

$$\zeta \approx \frac{1}{3} \left( \frac{1 + 2k_{\perp}^2 R_p^2}{1 + k_{\perp}^2 R_p^2} \right). \quad (35)$$

The parallel diffusion strength  $\alpha$  was always assumed to be equal to the perpendicular diffusion strength  $\gamma$ . The analytic expression for  $g(y)$  does not take account of cyclotron damping at high values of  $y$ , which implies that the computed proton heating rates should be considered upper limits.

Figure 4 displays various quantities in wavenumber space for the baseline model that assumes  $\alpha = \beta = \gamma = 1$  and  $(\delta U/\rho)^{1/2} = 50 \text{ km s}^{-1}$ . Contours of the proton and electron damping rates (dimensionless ratios  $|\omega_{i,s}/\omega_r|$ , for  $s = p, e$ ) were computed in the same manner as the curves in Figures 2 and 3, separated into proton and electron contributions using eq. (30), and plotted in Figure 4a. In Figure 4a we also give indications of the angle  $\theta$  between the background magnetic field and the wavevector. Note that significant proton cyclotron damping occurs (for Maxwellian proton distributions) only when  $k_{\parallel}$  exceeds the inverse inertial length  $\Omega_p/V_A$ , with a rapid, Gaussian decline for smaller values of  $k_{\parallel}$ . The onset of electron Landau damping, on the other hand, occurs much more gradually in the high- $k_{\perp}$  KAW limit.

Figure 4b shows contours of  $W(\mathbf{k})$ , computed as described above, and the critical balance ( $y = 1$ ) curve. Although the decay of fluctuation energy as a function of  $k_{\parallel}$  is steep, there is some residual energy that seems to make it to the proton cyclotron frequency. We should note, however, that for the case plotted in Figure 4b the solutions for  $k_{\parallel} V_A/\Omega_p \gtrsim 10^{-2}$  are only approximate. The explanation for the power-law behavior of  $g(y)$  at large values of  $y$  depends on the existence of perpendicular wavenumber diffusion from high  $k_{\perp}$  to low  $k_{\perp}$ . As can be seen in Figure 4b, there is sufficient Alfvénic power available to be perpendicularly diffused only for  $k_{\parallel} V_A/\Omega_p \lesssim 10^{-2}$  (i.e., to the right of the  $y = 1$  curve), and the extension of the power law to larger values of  $k_{\parallel}$  is an assumption that needs to be investigated further. We speculate that the inclusion of other (non-Alfvén) modes at higher values of  $k_{\perp}$  could make more power available to be diffused over a larger range of  $k_{\parallel}$ .

The integration of eq. (34) provides the individual heating and acceleration rates. Below, we express these

rates (i.e.,  $Q_{\parallel s}$  and  $Q_{\perp s}$ ) dimensionlessly by dividing them by a fiducial empirical value  $Q_{\text{emp}} \equiv 10^{-8} \text{ erg cm}^{-3} \text{ s}^{-1}$ , which is representative of required heating rates at  $2 R_{\odot}$  in various published models (e.g., Leer et al. 1982; Esser & Habbal 1995; Li et al. 1999; Dmitruk et al. 2002). For the baseline model illustrated in Figure 4, the dominant dissipation channel is Landau damping, which is converted mainly into parallel electron heating. In this model,  $Q_{\parallel e}/Q_{\text{emp}} = 0.26$ , and  $Q_{\perp e}$  is identically zero. There is a small amount of high- $k_{\parallel}$  cyclotron energization, which heats protons in the perpendicular direction ( $Q_{\perp p}/Q_{\text{emp}} = 9.1 \times 10^{-5}$ ) and cools them slightly in the parallel direction ( $Q_{\parallel p}/Q_{\text{emp}} = -1.9 \times 10^{-5}$ ). These rates, though, are far too small to provide the required energy to protons in the extended corona.

We performed a number of rate calculations with different values for  $\beta$ ,  $\gamma$ , and  $\delta U$ . The total heating rates scale closely with the injected cascade rate  $\varepsilon_0 \sim (\delta U/\rho)^{3/2}$ . Depending on the ratio  $\beta/\gamma$ , though, as much as 30% of the input cascade energy can be unaccounted for in the total Alfvén-wave damping. This is not surprising because we cut off the wave spectrum abruptly when the Alfvén branch solutions disappear and did not follow the flow of “mode-coupled” energy to higher wavenumbers. Following the complete turbulent cascade of energy on more than one dispersion branch is an important subject for future work.

The following phenomenological scaling relations were produced as empirical fits to the numerical results found by varying  $\beta$ ,  $\gamma$ , and  $\delta U$ :

$$\frac{Q_{\parallel e}}{Q_{\text{emp}}} \approx 0.22 \left[ \frac{(\delta U/\rho)^{1/2}}{50 \text{ km s}^{-1}} \right]^3 \left( \beta + \frac{2\gamma}{3} \right)^{1/3} \quad (36)$$

$$\frac{Q_{\perp p}}{Q_{\text{emp}}} \approx 9.1 \times 10^{-5} \left[ \frac{(\delta U/\rho)^{1/2}}{50 \text{ km s}^{-1}} \right]^{2n+1} y_{\text{res}}^{3.5-2n}. \quad (37)$$

The electron heating rate is relatively insensitive to the adopted values of  $\beta$  and  $\gamma$ , and its absolute value agrees with the empirically constrained total heating rate (i.e.,  $Q_{\parallel e} = Q_{\text{emp}}$ ) if  $(\delta U/\rho)^{1/2} \approx 120 \text{ km s}^{-1}$ .

Note the sensitive dependence of the proton heating rate on the exponent  $n$  in the power-law tail of  $g(y)$ . In the MHD inertial range,  $n$  is given simply by  $1+(3\beta/4\gamma)$ . The baseline case of  $\beta = \gamma$  sets the normalization in the exponent above (i.e., for this case  $2n = 3.5$ ). The dimensionless factor  $y_{\text{res}}$ , which we constrained by fitting to be

about 770, gives a rough indication of how far out in the tail the cyclotron interaction occurs. For proton heating, the dominant contribution to the integral in eq. (34) occurs when  $k_{\parallel} \approx k_{\perp}$  (i.e., when  $k_{\perp} R_p \approx 0.2$  at the proton cyclotron resonance) and at this wavenumber,  $y \approx 10^3$ .

Figure 5 plots the perpendicular proton heating rates from eq. (37) versus the ratio  $\beta/\gamma$ . Also plotted is a range of empirical proton heating rates from Li et al. (1999) that produce agreement with UVCS/SOHO H I Ly $\alpha$  observations. It is clear that if  $\beta = \gamma$ , one would need unrealistically high values of the total wave power to agree with the empirical rates. However, the required levels of wave power are greatly reduced if  $\gamma > \beta$ . For example, Esser et al. (1999) derived an empirical range of 110 to 130 km s $^{-1}$  for the total Alfvén wave velocity amplitude at  $2 R_{\odot}$ , using wave action conservation and spectroscopic limits on the base amplitude. To reach the empirical range of proton heating rates in Figure 5 simultaneously with this constraint on  $(\delta U/\rho)^{1/2}$ , one would need  $\gamma$  to be greater than, or of the same order as,  $\sim 4\beta$ . This does not seem to be an unreasonable condition on the turbulent cascade, but only simulations or laboratory experiments can provide firm limits on how the effective advection and diffusion strengths compare with one another.

The use of  $\delta U$  as a total wave energy quantity glosses over the fact that, at the outer scale, there is probably considerably more power in outward-propagating waves ( $k_{\parallel} > 0$ ) than in inward-propagating waves ( $k_{\parallel} < 0$ ). Let us compare the heating rates computed above with the turbulence model of Matthaeus et al. (1999) and Dmitruk et al. (2001, 2002), who took the asymmetry in the outward and inward populations into account. Their net heating rate can be expressed as

$$Q \approx \rho \frac{Z_-^2 Z_+ + Z_+^2 Z_-}{L_{\text{out}}} \quad (38)$$

where  $Z_-$  and  $Z_+$  are wavenumber-integrated Elsässer amplitudes (with velocity units) of outward and inward propagating fluctuations, respectively, and  $L_{\text{out}}$  is a representative energy-containing length scale. Dmitruk et al. (2001, 2002) also approximated the reflected inward power  $Z_+$  as  $\sim L_{\text{out}} |\partial V_A / \partial r|$ . For the parameters at  $2 R_{\odot}$  discussed in § 3.1, the outer scale  $L_{\text{out}}$  assumed in our cascade equation, and  $Q = Q_{\text{emp}}$ , we solve for  $Z_-$  and  $Z_+$  to be approximately 30 and 7 km s $^{-1}$ , respectively. These quantities are amplitudes most comparable

to the peak value of  $W_{\perp}^{1/2}$  at the outer scale, so in order to compare them with  $(\delta U/\rho)^{1/2}$  we must multiply by the factor of 5 that arises because of the broadening of  $W_{\perp}$  as a function of  $k_{\perp}$  (see § 2.2). This implies a total outward wave power equivalent to  $(\delta U/\rho)^{1/2} \approx 150$  km s $^{-1}$ , which is close to the empirical range reported by Esser et al. (1999). Our requirement above that  $(\delta U/\rho)^{1/2}$  must be of order 120 km s $^{-1}$  is also within this range. Thus, although we did not consider outward/inward asymmetries explicitly, the derived requirements on the total wave power seem robust and useful nonetheless.

It is still uncertain whether the dissipation of Alfvénic turbulence in the extended corona will preferentially heat electrons or protons. If van Ballegooijen’s (1986) statistical limit of  $\beta = \gamma$  holds for actual strong MHD or KAW turbulence, it seems clear that the electrons will be primarily heated along the magnetic field and there would not be sufficient wave power at the ion cyclotron frequencies to heat protons and heavy ions. This represents a problem when confronted with spectroscopic observations of extreme ion heating and anisotropy (with  $T_{\perp} \gg T_{\parallel}$ ) and at least mild preferential heating of protons over electrons (e.g., Kohl et al. 1996, 1997, 1998; Esser et al. 1999; Cranmer et al. 1999b; Doschek et al. 2001). We discuss alternate ways of energizing protons and heavy ions in the extended corona below in §§ 4–5.

#### 4. Nonlinear Evolution of Electron Beams

Here we explore the possible consequences of the strong (but largely unobserved) parallel electron heating that would be the result of Landau damping of kinetic Alfvén waves. The ideas discussed in this section are considerably more speculative than those discussed above, but we are guided by detailed *in situ* observations of roughly similar conditions in the Earth’s ionosphere and magnetosphere. We gratefully acknowledge Matthaeus et al. (2003a, 2003b) for the initial suggestion that the following empirical constraints in near-Earth plasma environments could be applied to the solar corona and solar wind.

A possible sequence of events could progress as follows. The Landau damping of Alfvén waves heats electrons in the parallel direction and has been shown, if allowed to develop far enough, to lead to non-Maxwellian

tails (Tanaka, Sato, & Hasegawa 1987, 1989; Leubner 2001). These effectively beamed distributions may be unstable to the direct generation of ion cyclotron waves (Markovskii & Hollweg 2002) which could heat protons. However, we also note that electron velocity distributions with monotonically decreasing tails may eventually develop into non-monotonic bump-in-tail distributions if the processes that accelerate electrons are intermittent or otherwise spatially localized (e.g., Cairns 1987). Even weak bump-in-tail electron beams have been shown to easily generate parallel Langmuir waves via various plasma instabilities (e.g., Thompson 1971; Melrose & Goldman 1987; Dum 1990; and references therein). Evolved Langmuir wave trains exhibit a periodic electric potential-well structure in which some of the beam electrons can become trapped. Adjacent potential wells can eventually merge with one another and gradually form isolated “holes” of saturated potential in electron phase space (Krasovsky, Matsumoto, & Omura 1999; Omura et al. 2001; Mottez 2001).

Electron phase-space holes (EPHs) are equilibrium electrostatic structures that have been predicted to exist for some time (Bernstein, Greene, & Kruskal 1957) and have been observed in the last decade in space plasma environments where electrons are accelerated along the background magnetic field (e.g., Matsumoto et al. 1994; Ergun et al. 1998, 1999; Bale et al. 1998, 2002). The traditional formation mechanism for EPHs has long been considered to be the two-stream instability, but the observed EPHs have potential amplitudes that are too small to be formed from the strong counter-streaming electron beams required to excite this instability. The above bump-in-tail/Langmuir excitation scenario is an alternate mechanism that has been shown to be able to form EPHs in numerical simulations. The stochastic nature of MHD turbulence (possibly dissipating in small reconnection sites) has also been shown to lead to similar kinds of intermittent nonlinearities (Dupree 1982; Ambrosiano et al. 1988; Biglari & Diamond 1989; Marsch, Tu, & Rosenbauer 1996; Tu, Marsch, & Rosenbauer 1996; Drake et al. 2003).

The reason we consider the effects of EPHs in the context of this paper is that in many places where phase-space holes are observed (e.g., Ergun et al. 1998), protons exhibit preferential heating in the direction perpendicular to the magnetic field. Ergun et al. (1999) sug-

gested that EPHs act as quasi-particles whose positively charged cores repel ions in a manner similar to ion-ion Coulomb collisions. Under certain conditions, a large number of these stochastic collisions can lead to ion heating. Because EPHs tend to flow along the magnetic field at velocities of order the electron most-probable speed ( $w_{\parallel e} \sim 5000 \text{ km s}^{-1}$  in the extended corona), the ions are roughly sitting still as the EPHs flow by. The net impulses the ions receive would thus be in the perpendicular direction. Below, we work out a quantitative estimate for the perpendicular heating experienced by protons in the extended corona due to EPH quasi-collisions.

#### 4.1. Phase Space Hole Properties

Consider a homogeneous proton-electron plasma with the following localized disturbance in the electrostatic potential:

$$\Phi(x, y, z) = \Phi_0 \exp \left[ - \left( \frac{z}{z_0} \right)^2 - \left( \frac{r}{r_0} \right)^2 \right], \quad (39)$$

where the  $z$  direction is that of the background magnetic field and  $r^2 = x^2 + y^2$ . The equipotential surfaces are oblate spheroids centered around the origin, and the above distribution is in agreement with several analyses of isolated EPH properties (e.g., Turikov 1984; Chen & Parks 2002). The parallel length scale  $z_0$  has been observed in several space plasmas to be of the same order of magnitude as the electron Debye length, and we define

$$z_0 \equiv \frac{\delta \lambda_D}{2} \quad (40)$$

where  $\lambda_D = w_{\parallel e}/\omega_{pe}\sqrt{2}$  is the electron Debye length and  $\delta$  is a dimensionless number that is observed to be typically 2 to 3. (Ergun et al. 1998). The transverse length scale  $r_0$  may scale with the proton gyroradius in regions where  $\Omega_e/\omega_{pe} \gg 1$ , but Franz et al. (2000) estimated that

$$\frac{r_0}{z_0} \approx \left( 1 + \frac{\omega_{pe}^2}{\Omega_e^2} \right)^{1/2} \quad (41)$$

in regions where  $\Omega_e/\omega_{pe} \ll 1$  (which is more applicable to the solar corona). The above relation, which we apply in the model below, gives an aspect ratio  $r_0/z_0$  of about 3 to 10 in the extended corona.

The localized electric field resulting from the above potential can be determined analytically ( $\mathbf{E} = -\nabla\Phi$ ), and the charge density distribution is found by applying Coulomb’s law. The full analytic expression for the charge density  $\rho^*(r, z)$  agrees with the plots in Figure 3b of Ergun et al. (1998), who modeled two extreme examples of EPH geometry by effectively assuming  $r_0 = z_0$  (“sphere”) and  $r_0 \gg z_0$  (“plane”). There is a net positive charge density in the central core of the EPH which is surrounded by a net negative charge density. The positive charge density at the center of the EPH (i.e., at  $r = 0$ ,  $z = 0$ ) is expressible in terms of the difference between local proton and electron number densities,

$$\delta n \equiv n_p - n_e = \frac{\Phi_0}{2\pi e} \left( \frac{2}{r_0^2} + \frac{1}{z_0^2} \right), \quad (42)$$

which can be simplified further by neglecting the first term in the parentheses (because  $r_0 \gg z_0$ ). In this limit, we can express the ratio of  $\delta n$  to the total electron density  $n_e$  as

$$\frac{\delta n}{n_e} = \frac{16}{\delta^2} \frac{(e\Phi_0/m_e)}{w_{\parallel e}^2}. \quad (43)$$

This allows us to convert between the central potential  $\Phi_0$  and the central charge separation  $\delta n$ .

We assume the EPH moves along the  $z$  direction with speed  $v_H$ . This speed will probably be of the same order as the parallel electron thermal speed, so let us follow Turikov (1984) and define the Mach number  $M \equiv v_H/w_{\parallel e}$ . Turikov (1984) found that one-dimensional EPHs become unstable and break up when  $M > 2$ , and Ergun et al. (1998) report values of  $M$  between  $\sim 0.2$  and 2 in the ionosphere. One cannot arbitrarily choose all three of the quantities  $\delta$ ,  $M$ , and  $\delta n/n_e$ . They are interrelated by the constraint that the electrons obey the Vlasov equation and can self-consistently affect the electric potential via Poisson’s equation. Turikov (1984) computed a relation that allows us to solve for  $\delta n/n_e$  as a function of  $\delta$  and  $M$ . For a Gaussian potential in the  $z$  direction (eq. [39]) and a weak charge separation (i.e.,  $\delta n/n_e \ll 1$ , which always seems to hold for reasonable values of the parameters),

$$\frac{\delta n}{n_e} \approx \left( \frac{\delta}{\delta_0} \right)^4 e^{-2M^2} \quad (44)$$

where  $\delta_0 = 4\pi^{-1/4}(2\ln 4 - 1)^{1/2}$  for the Gaussian potential. Coincidentally, this value of  $\delta_0$  is extremely close to

a value of 4.0. Chen & Parks (2001) noted that the above relation is formally only an upper limit on  $\delta n/n_e$ , but it is a useful scaling relation that we will assume holds for EPHs in the corona. Note from eqs. (43) and (44) that the central potential  $\Phi_0$  is proportional to  $\delta^6$ , and thus is extremely sensitive to the parallel size of the EPH.

One additional quantity that needs to be constrained is the spatial number density of EPHs—or equivalently, their filling factor—in the plasma. Only a detailed analysis of EPH formation will yield constraints on how frequently they appear in space after significant merging has occurred, so here we use empirical limits from the *in situ* measurements. Defining the volume of an EPH as the equipotential surface that is  $1/e$  times its central potential, we relate their spatial number density  $n_H$  to their fractional filling factor  $f_H$  via

$$n_H = \frac{f_H}{4\pi z_0 r_0^2/3}. \quad (45)$$

In a field of highly oblate EPH structures moving in the  $z$  direction,  $f_H$  can be estimated by analyzing the mean time (or distance) between significant electric-field “kicks” felt by a slowly moving observer. For EPHs distributed randomly in three-dimensional space,  $f_H$  should be close to the ratio  $z_0/\Delta z$ , where the denominator is the mean distance between strong EPHs in the  $z$  direction. Ergun et al. (1998) found that there are often times when  $\Delta z \approx v_H/\Omega_p$ , which we use in the rough calculations below. The specification for the filling factor also must take account of electron-electron Coulomb collisions, because if these collisions occur on a time scale *faster* than the time it takes to Landau-damp the MHD turbulence and build up electron beams, then EPHs should not form at all. Thus, let us modify the purely geometric filling factor by an approximate collision term, with

$$f_H \approx \frac{z_0\Omega_p}{v_H} \frac{1}{1 + (\tau_{\text{diss}}/\tau_{\text{coll}})^2} \quad (46)$$

where  $\tau_{\text{diss}}$  is a turbulence dissipation time scale that we approximate as  $L_{\text{out}}/Z_-$  (eq. [38]) and is about 200 s for  $(\delta U/\rho)^{1/2} \approx 100 \text{ km s}^{-1}$  (see § 3.2). The standard electron self-collision time is

$$\tau_{\text{coll}} \approx \frac{0.266 T_e^{3/2}}{n_e \ln \Lambda} \quad (47)$$

(Spitzer 1962), where we assume  $\ln \Lambda = 21$ . When  $\tau_{\text{coll}} \ll \tau_{\text{diss}}$  the EPH filling factor approaches zero, and

when  $\tau_{\text{coll}} \gg \tau_{\text{diss}}$  the filling factor approaches the value constrained by Ergun et al. (1998). For plasma conditions at  $2 R_{\odot}$ , we can use canonical values of  $\delta = 3$  and  $M = 1$  to estimate  $f_{\text{H}}$  to be  $\sim 10^{-4}$ , implying a spatial number density of  $3 \times 10^{-10} \text{ cm}^{-3}$ .

## 4.2. Quasi-Collisions and Proton Heating

A single electron phase-space hole moving along the  $z$  direction encounters a positive ion (with mass  $m_i$  and charge  $q_i$ ) at a perpendicular impact parameter, or distance of closest approach, denoted by  $r$ . We ignore Lorentz forces along the  $z$  direction because they are expected to roughly cancel out between the approaching and receding halves of the EPH trajectory. The perpendicular momentum given to the ion over the entire trajectory is given by

$$m_i \Delta v_{\perp i} = \int_{-\infty}^{+\infty} dt q_i E_{\perp}(t) , \quad (48)$$

where the time  $t$  and the relative parallel displacement  $z$  between the EPH and the ion are related simply by  $z = v_{\text{H}} t$ . The perpendicular electric field felt by the ion is that of the isolated EPH potential,

$$\begin{aligned} E_{\perp} &= (E_x^2 + E_y^2)^{1/2} \\ &= \frac{2r\Phi_0}{r_0^2} \exp \left[ - \left( \frac{v_{\text{H}} t}{z_0} \right)^2 - \left( \frac{r}{r_0} \right)^2 \right] . \end{aligned} \quad (49)$$

We thus compute the perpendicular velocity impulse analytically to be

$$\Delta v_{\perp i} = \frac{2\pi^{1/2} q_i r \Phi_0 z_0}{m_i r_0^2 v_{\text{H}}} \exp \left[ - \frac{r^2}{r_0^2} \right] . \quad (50)$$

Following the standard development of Coulomb collision rates (e.g., Spitzer 1962; Jackson 1975), we extend the above calculation from one EPH to a “field” of EPHs distributed throughout space with number density  $n_{\text{H}}$ . The number of ion/EPH encounters per unit time with impact parameters between  $r$  and  $r + dr$  is given by  $(2\pi r dr v_{\text{H}} n_{\text{H}})$ . The effective *diffusion coefficient* for perpendicular energization of the ion by the field of EPHs is then given by

$$\mathcal{D}_{\perp i} \equiv \frac{d(\Delta v_{\perp i}^2)}{dt} = \int_0^{\infty} dr 2\pi r v_{\text{H}} n_{\text{H}} (\Delta v_{\perp i})^2$$

$$= \frac{\pi^2 n_{\text{H}} q_i^2 \Phi_0^2 z_0^2}{m_i^2 v_{\text{H}}} . \quad (51)$$

Because of the exponential dependence of  $E_{\perp}$  as a function of  $r$ , the above integral was well-defined and finite over all values of the impact parameter. This is a relative simplification over the ion-ion Coulomb collision problem, where the above integral formally diverges and must be truncated using a maximum impact parameter.

In the limit of a field of very low-energy ions,  $\mathcal{D}_{\perp i}$  is essentially the heating rate per particle, per unit mass. As the ions heat up, however, the amount of energy they extract from the EPHs cannot be arbitrarily large. Ideally, we should solve coupled energy conservation equations for both ions and EPHs, where each equation would contain energy exchange terms that would eventually lead to equipartition. It is not clear, though, how much of the EPH energy is actually “disposable” (i.e., easily given away to ions in collision-like interactions).

In the frame at rest with respect to a phase-space hole, its electrostatic potential energy is given by the following volume integration,

$$U_{\text{E}} = \int d^3 \mathbf{x} \frac{|\mathbf{E}|^2}{8\pi} = \frac{\Phi_0^2}{8} \sqrt{\frac{\pi}{2}} \left( \frac{r_0^2}{2z_0} + z_0 \right) , \quad (52)$$

which is considerably larger than the kinetic energies of individual protons or electrons in the solar corona. In the frame of an ion, the EPH is moving by at a relatively high speed (though we assume  $v_{\text{H}} \ll c$ ), and an induced perpendicular magnetic field is felt by the ion with a potential energy given by

$$U_{\text{B}} = \frac{v_{\text{H}}^2}{c^2} \int d^3 \mathbf{x} \frac{|E_{\perp}|^2}{8\pi} = \frac{\Phi_0^2}{8} \sqrt{\frac{\pi}{2}} \frac{z_0 v_{\text{H}}^2}{c^2} \quad (53)$$

which is several orders of magnitude smaller than the total electrostatic energy of the EPH. The induced magnetic energy is proportional to  $v_{\text{H}}^2$  and seems to be analogous to a kind of kinetic energy. Our conjecture is that  $U_{\text{B}}$  represents an order-of-magnitude estimate for the energy available to be given away by EPHs in collisions with ions. We express this energy quantity as an equivalent temperature ( $U_{\text{B}} \equiv k_{\text{B}} T_{\text{B}}$ ) and insert the adopted conditions at  $2 R_{\odot}$  (i.e.,  $\lambda_D = 14 \text{ cm}$  and  $w_{\parallel e} = 5700 \text{ km s}^{-1}$ ) to obtain

$$T_{\text{B}} \approx (4.3 \times 10^{12} \text{ K}) \left( \frac{\delta}{\delta_0} \right)^{13} M^2 e^{-4M^2} \quad (54)$$

(see, e.g., eqs. [43] and [44]). For increasing  $M$ , the total magnetic energy in the EPH begins to decrease above about  $M \approx 0.2$  because very fast EPHs contain fewer trapped electrons and thus cannot support as high a potential as a slower EPH.

In the extended corona, the value of  $T_B$  is huge in comparison to individual particle temperatures. Further, this large value of  $T_B$  is *smaller* by at least a factor of  $v_H^2/c^2$  than the temperature quantity equivalent to the total electrostatic energy of a phase-space hole. EPHs seem to embody a substantial “pool” of energy that is continually replenished by KAW turbulence and Landau damping, and this energy does not seem to be diminished significantly by collisions with ions. Thus, we do not consider the approach to energy equipartition any further and assume that eq. (51) gives the effective net ion heating rate per unit mass.

For the specific case of protons, we solve a steady-state solar wind internal energy conservation equation with the EPH diffusion coefficient as the sole source of extended heating. Our approach ignores the impact of heat conduction and energy sharing via particle-particle collisions, but these effects are expected to be relatively weak in the extended corona (e.g., Olsen & Leer 1996; Li 1999). We thus assume that the proton perpendicular temperature  $T_{\perp p}$  evolves with radius according to

$$u_{\parallel p} \left( \frac{\partial T_{\perp p}}{\partial r} + \frac{T_{\perp p}}{A} \frac{\partial A}{\partial r} \right) = \frac{m_p \mathcal{D}_{\perp p}}{2k_B}, \quad (55)$$

where  $u_{\parallel p}(r)$  is the time-steady outflow speed profile and  $A(r)$  is the cross-sectional area of a solar wind flow tube. The second term in parentheses above is responsible for adiabatic proton cooling due to the geometric expansion of the plasma. Empirically determined values for the radial dependences of  $u_{\parallel p}$ ,  $A$ ,  $n_e$ ,  $B_0$  (the background magnetic field strength), and  $T_e$  (the electron temperature; needed to compute  $\lambda_D$ ) are elaborated by Cranmer, Field, & Kohl (1999a). We integrate eq. (55) from an inner boundary at the base of the corona to an outer boundary in the extended corona. The remaining free parameters are the inner boundary value of  $T_{\perp p}$  and the EPH parameters  $\delta$  and  $M$ , which we assume to be constant in the extended corona. We assume the EPH filling factor  $f_H$  is given by eq. (46).

Figure 6a shows the effective heating rate  $Q_{\perp p} \equiv \rho \mathcal{D}_{\perp p}/2$ , computed using eqs. (43–47) and eq. (51), for

various values of  $\delta$  and a fixed value of  $M = 1$ . It also plots  $Q$  for the Dmitruk et al. (2001, 2002) turbulence dissipation rate (eq. [38]), with the radial dependence  $\rho Z_-^2 \propto V_A(u_{\parallel p} + V_A)^{-2} A^{-1}$  given by wave action conservation (see also Zank, Matthaeus, & Smith 1996). We interpret the order-of-magnitude similarity of the two sets of rate quantities as a promising plausibility argument for EPH proton heating. Despite this similarity, though, the two sets of rates are essentially “apples and oranges,” since the Dmitruk et al. values come solely from the turbulent cascade rate and the EPH values do not contain any information about the cascade. The EPH curves in Figure 6a are not energetically consistent with the turbulence because we use the empirical filling factor  $f_H$  discussed above. A more self-consistent model of EPH heating would follow the turbulent energy budget from the dissipation by Landau damping to the growth of electron beams (which would embody only a fraction of the total dissipated energy) to the eventual intermittent formation of EPHs.

For protons that start out with  $T_{\perp p} = 10^6$  K at  $r = 1.25 R_{\odot}$  (assuming some collisional contact with electrons), Figure 6b plots the computed radial dependence of  $T_{\perp p}$  for the same range of  $\delta$  values as in Figure 6a. (The temperature curves are similar to those computed for a single value of  $\delta$  and a range of  $M$  values.) Substantial proton heating is evident, but the results are very sensitive to the values of the EPH parameters. It would probably be more realistic to assume distributions of  $\delta$  and  $M$  (see, e.g., Figure 4a of Ergun et al. 1998), but this introduces free parameters as well. Note, though, that the mean value of  $\delta$  reported by Ergun et al. (1998) is  $\sim 3.6$ , which is closest to the value that would give  $T_{\perp p}(r)$  most similar to the UVCS H I empirical model results (Kohl et al. 1998).

The proton heating models shown in Figure 6 are suggestive but nowhere near conclusive. A major source of uncertainty is the application of the ionospheric EPH spacing relation  $\Delta z = v_H/\Omega_p$  to the calculation of the EPH filling factor in the corona. This could be different by orders of magnitude, which would significantly change the above results. Also, our assumptions that  $\delta$  and  $M$  are constant with radius and that eq. (44) gives the exact central EPH potential should be examined critically. More work should be devoted toward investigating the growth and development of EPHs in the corona,

as well as their interactions with protons, heavy ions, and the “untrapped” electrons.

## 5. Discussion and Conclusions

In this paper we suggested two alternative “channels” by which protons and other positive ions in the extended solar corona can be heated perpendicularly to the background magnetic field (see Figure 7). First, the parallel decay of anisotropic MHD turbulence to ion cyclotron frequencies may occur if the cascade is properly modeled by advection and diffusion strengths  $\beta$  and  $\gamma$  with the property  $\gamma \gtrsim 4\beta$ . This result could lend some support to the many other proposed models that describe the damping of parallel-propagating ion cyclotron waves in a coronal context. (Note, however, that many more issues, such as implementing a more self-consistent cascade and damping formalism at large values of  $k_{\parallel}$ , still needs to be resolved). Second, we proposed that, if  $\gamma < 4\beta$ , the dominant parallel electron heating associated with KAW Landau damping could lead to the nonlinear generation of electron phase-space holes. These EPHs have been shown to undergo collision-like interactions with positive ions and heat them mainly perpendicularly. The EPH idea is extremely speculative because as yet we have no quantitative constraint on their spatial filling factor in the corona. Only if they are generated in sufficient numbers (i.e., only if the conversion from KAWs to electron beams to EPHs is efficient enough) can they provide substantial proton heating.

There are several other related mechanisms by which protons and heavy ions could be heated in the extended corona. If there is substantial power in obliquely propagating fast-mode magnetosonic waves, their collisionless damping may contribute to proton heating (e.g., Li & Habbal 2001; Hollweg & Markovskii 2002). Oblique Alfvén and fast-mode waves can steepen into shocks under certain conditions, and numerical simulations that employ the derivative nonlinear Schroedinger equation (DNLS) have produced a rich variety of steepening phenomena that produce power at high-frequency harmonics of an input spectrum (e.g., Spangler 1997). Certain types of collisionless shocks may also accelerate ions in the direction perpendicular to the magnetic field (Lee & Wu 2000). The basal generation and “sweeping” of high-

frequency waves (e.g., Axford & McKenzie 1992; Tu & Marsch 1997) must also be developed further to determine to what degree these waves can survive in the extended corona (see also Cranmer 2001). Because of the multiplicity of time and spatial scales involved in studying many of these processes, the dominant physics may become evident only when a large number of competing mechanisms are included together in a solar wind model and allowed to evolve self-consistently.

The proton heating that arises from ion cyclotron wave dissipation depends sensitively on the shape of the proton velocity distribution function. We assumed Maxwellian distributions in the above analysis, and the conclusions are not affected strongly if there is moderate bi-Maxwellian anisotropy. If the protons have suprathermal high-energy tails (e.g., Scudder 1992), though, the resonance function  $\mathcal{R}_s$  would have a less steep frequency dependence compared to eq. (32). In this case, waves with lower  $k_{\parallel}$  would be included in the thermally broadened ion cyclotron resonance and thus lead to a lower effective value of  $y_{\text{res}}$  in eq. (37). For strong enough suprathermal tails, it is possible that even the baseline cascade model (with  $\beta = \gamma$ ) could contain enough parallel decay of wave energy to heat protons substantially. It should be noted, however, that Isenberg (2003) concluded from a completely collisionless description of “kinetic shell” velocity distributions that the damping of parallel-propagating ion cyclotron waves is not a likely source of proton heating even if there is sufficient wave power in the extended corona. Indeed, damping rates for the non-Maxwellian distributions predicted in quasi-linear models of collisionless resonant heating can be substantially different than those computed for Maxwellians (e.g., Isenberg 2001; Cranmer 2001; Tu & Marsch 2002). Full kinetic models that follow the protons and electrons from the collisional low corona to the collisionless extended corona are needed to resolve these issues.

Some mention should be made of the effects of heavy ions on the above analysis. It has been clear for several decades that the 5% to 10% abundance of  $\text{He}^{2+}$  in the corona is responsible for a strong resonance in the Alfvén wave dispersion relation, but it is unclear whether the other thousands of minor ion species are numerous enough to affect the dispersion relation (Isenberg 1984; Gomberoff, Gratton, & Gnani 1996). Mode coupling be-

tween the different branches must be modeled explicitly in order to determine how much wave power survives at the proton cyclotron resonance. Also, it should be made clear that the EPH quasi-collision mechanism proposed above is *not* an efficient source of preferential heating for heavy ions, even if it is able to supply sufficient heat to the protons. The effective ion heating rate is proportional to  $m_i \mathcal{D}_{\perp i}$ , which scales with charge and mass as  $q_i^2/m_i$  (eq. [51]). The  $O^{5+}$  ions measured by UVCS/SOHO in the extended corona have a perpendicular kinetic temperature about two orders of magnitude larger than that of protons. The EPH mechanism, though, would only provide an oxygen temperature larger than the proton temperature by a factor of  $5^2/16 \sim 1.6$ . The damping of ion cyclotron waves still seems to be the most likely source of preferential heating and acceleration for heavy ions.

Improvements in remote-sensing measurements of the extended solar corona are needed to make significant further progress in identifying and characterizing the most important physical processes. Next-generation spectroscopic instruments are being designed with the capability to sample the velocity distributions of dozens of ions in the acceleration region of the high-speed wind,

as opposed to just 2–3 ions with UVCS. In addition to being sensitive to many more emission lines, these instruments could also detect subtle departures from Gaussian line shapes that constrain the presence of specific non-Maxwellian distributions (e.g., Cranmer 1998, 2001). Seldom-used diagnostics such as the measurement of the Thomson scattered H I Ly $\alpha$  profile (which probes the line-of-sight electron velocity distribution; see Withbroe et al. 1982) can put firm constraints on both the “core” electron temperature and the existence of beam-like or power-law wings. Improvements in radio sounding observations are also making it possible to extract a great deal of information about MHD turbulence in the solar wind (e.g., Spangler 2002).

The authors would like to thank William Matthaeus, Jack Scudder, George Field, and S. Peter Gary for valuable and inspiring discussions. This work is supported by the National Aeronautics and Space Administration under grants NAG5-11913 and NAG5-11420 to the Smithsonian Astrophysical Observatory, by Agenzia Spaziale Italiana, and by the Swiss contribution to the ESA PRODEX program.

### A. The Advection-Diffusion Cascade Model

This Appendix provides details concerning the solution of eqs. (11) and (12). The two-dimensional advection-diffusion cascade model (eq. [11]) can be simplified by defining the following supplementary variables:

$$\widetilde{W}(k_{\perp}) \equiv W_{\perp}^{3/2} k_{\perp}^{-3\beta/2\gamma} \quad (A1)$$

$$F(k_{\perp}) \equiv \frac{2\gamma}{3} \phi_e^{1/2} k_{\perp}^{2+(3\beta/2\gamma)} . \quad (A2)$$

We thus can define the perpendicular cascade rate  $\varepsilon$  as

$$\varepsilon(k_{\perp}) \equiv -F(k_{\perp}) \frac{\partial \widetilde{W}}{\partial k_{\perp}} , \quad (A3)$$

which in the MHD regime ( $\phi_e = 1$ ) is proportional to  $k_{\perp} v_{\perp}^3$ . With the above definitions, eq. (11) simplifies to

$$\frac{\partial W_{\perp}}{\partial t} = -k_{\perp} \frac{\partial \varepsilon}{\partial k_{\perp}} + S(k_{\perp}) - D(k_{\perp})W_{\perp} . \quad (A4)$$

In the inertial range, where both  $S$  and  $D$  are negligibly small, it is easy to see that the time-steady solution exhibits a constant value of  $\varepsilon$ , which we will denote  $\varepsilon_0$ . This cascade rate is supplied by the source function  $S(k_{\perp})$ , which we estimate to have the following Gaussian shape:

$$S(x) = \frac{\varepsilon_0}{\pi^{1/2} \sigma_{\text{out}}} \exp \left[ - \left( \frac{x - x_{\text{out}}}{\sigma_{\text{out}}} \right)^2 \right] , \quad (A5)$$

where  $x = \ln k_\perp$  and  $x_{\text{out}} = \ln k_{\text{out}}$ . The dimensionless width of the Gaussian is given by  $\sigma_{\text{out}} = 1$  in all models presented in this paper. With this explicit form for  $S$ , the wavenumber dependence of the time-steady cascade rate (at wavenumbers where  $D \approx 0$ ) can be found by integrating eq. (A4), with

$$\varepsilon(x) = \frac{\varepsilon_0}{2} \left[ 1 + \operatorname{erf} \left( \frac{x - x_{\text{out}}}{\sigma_{\text{out}}} \right) \right] . \quad (\text{A6})$$

This provides a smooth transition from zero cascade (when  $k_\perp \ll k_{\text{out}}$ ) to cascade at the specified rate  $\varepsilon_0$  (when  $k_\perp \gg k_{\text{out}}$ ). Thus, the solution for  $\widetilde{W}$  in the inertial range can be computed straightforwardly via

$$\widetilde{W}(k_\perp) = \int_{k_\perp}^{+\infty} \frac{\varepsilon(k'_\perp) dk'_\perp}{F(k'_\perp)} . \quad (\text{A7})$$

When  $k_\perp \ll k_{\text{out}}$ , the cascade rate approaches zero and  $\widetilde{W}$  is constant, implying an energy spectrum  $W_\perp \propto k_\perp^{\beta/\gamma}$ . In the MHD inertial range,  $\varepsilon$  is equal to a constant value of  $\varepsilon_0$  and eq. (A7) can be integrated analytically to yield that  $W_\perp^{3/2}$  is proportional to  $k_\perp^{-1}$ . This results in the Kolmogorov-Obukhov spectrum  $W_\perp \propto k_\perp^{-2/3}$ . In the KAW inertial range,  $\phi_e \propto k_\perp^2$  and eq. (A7) integrates to obtain  $W_\perp \propto k_\perp^{-4/3}$ .

For the full range of  $k_\perp$  values below the dissipation range, the integration of eq. (A7) was performed numerically to obtain the undamped curve in Figure 1. For  $\phi_e$  given by eq. (9), an approximate “bridging solution” for the inertial range is

$$W_\perp(k_\perp) \approx \left( \frac{3\varepsilon_0}{2\gamma k_\perp} \right)^{2/3} \left[ \left( 1 + \frac{3\beta}{2\gamma} \right) \sqrt{1 + k_\perp^2 R_p^2} + k_\perp R_p \right]^{-2/3} \quad (\text{A8})$$

which is valid in the MHD and KAW inertial-range limits and differs by no more than 6% from the exact numerical solution when  $k_\perp R_p \approx 1$ . The above solution was used as the initial condition in the Crank-Nicholson finite difference code (e.g., Press et al. 1992) that included the effects of dissipation. All runs of the code reported in this paper utilized an evenly spaced grid in  $\ln k_\perp$ , spanning six orders of magnitude from  $k_\perp R_p = 10^{-3}$  to  $10^3$ . The portions of the wave spectrum below the minimum value of  $k_\perp$  were assumed to remain at the values given by the numerical integration of eq. (A7). The implicit nature of the finite-difference scheme allowed us to use a natural time step of 0.1 times the minimum value of  $\tau_s$  in the wavenumber grid. The system was evolved toward a steady state, and any numerical diffusivity was identified by simultaneously evolving the same spectrum both with ( $D \neq 0$ ) and without ( $D = 0$ ) damping. The latter case isolated long-time-scale numerical effects that were negligible in magnitude, but nevertheless divided out of the final damped spectrum.

An interesting feature of eqs. (11) and (A4) is that the behavior of the inertial range is largely independent of the values of  $\beta$  and  $\gamma$ . Indeed, even in the limit of pure advection (i.e.,  $\gamma = 0$ ), one can derive analytic solutions for the inertial range and the dissipation range. (Some of the supplementary quantities defined in this Appendix become undefined for  $\gamma = 0$ , but the original advection-diffusion equation remains well-defined.) For  $\gamma = 0$ , the rapid cutoff in the dissipation range is an explicit exponential decline (see, e.g., Townsend 1951; Pao 1965).

The remainder of this Appendix is devoted to the derivation of eq. (18), the analytic solution for  $g(y)$ . Beginning with the time-steady advection-diffusion equation (eq. [12]) in the inertial range ( $S = D = 0$ ), we substitute in the *ansatz* functional form for  $W(k_\perp, y)$  given in eq. (16). Then, to evaluate the partial derivatives with respect to  $k_\perp$ , we assume that  $W_\perp$  conforms to a local power-law form proportional to  $k_\perp^{-2\zeta}$  (as defined in eq. [20]). Even if  $\zeta$  is allowed to vary as a “slow” function of  $k_\perp$ , the dominant variation in  $W_\perp$  should remain the power-law decline with the local value of  $\zeta$ . This assumption allows  $\zeta$  to be considered constant as a function of  $y$ . After considerable but straightforward algebra, eq. (12) becomes the following ordinary differential equation with  $y$  as the independent variable:

$$(2\zeta - \eta) h(y) + (1 - \zeta) y h'(y) + \alpha g''(y) = 0 . \quad (\text{A9})$$

The supplementary quantity  $h$  is defined as

$$h(y) \equiv [\beta + \gamma(1 + \zeta)]g(y) + \gamma(1 - \zeta)y g'(y) , \quad (\text{A10})$$

and primes denote differentiation with respect to  $y$ . The dimensionless exponent  $\eta$  is defined as

$$\eta \equiv \frac{k_{\perp}}{2\phi_e} \frac{\partial\phi_e}{\partial k_{\perp}} \quad (\text{A11})$$

(i.e.,  $\eta = 0$  in the MHD inertial range and  $\eta = 1$  in the KAW inertial range). Serendipitously, the ratio

$$\frac{2\zeta - \eta}{1 - \zeta}$$

is equal to 1 in both the MHD and KAW inertial ranges. From numerical solutions of  $W_{\perp}$  and  $\phi_e$ , the above ratio is never less than 1 or larger than  $\sim 1.3$  in the narrow transition between the MHD and KAW inertial ranges. Thus, it seems reasonably safe to assume that this ratio is unity for all relevant wavenumbers, and we simplify eq. (A9) as

$$(1 - \zeta) [h(y) + y h'(y)] + \alpha g''(y) = 0 . \quad (\text{A12})$$

This equation is integrated once, assuming  $g'(0) = 0$ , to obtain the first-order differential equation

$$(1 - \zeta) y h(y) + \alpha g'(y) = 0 . \quad (\text{A13})$$

Inserting the definition of  $h(y)$ , we obtain the relatively simple equation

$$\frac{1}{g} \frac{dg}{dy} = \frac{-(1 - \zeta) [\beta + \gamma(1 + \zeta)] y}{\alpha + \gamma(1 - \zeta)^2 y^2} \quad (\text{A14})$$

which can be integrated analytically to obtain eq. (18). For the aforementioned case of pure perpendicular advection (i.e.,  $\gamma = 0$ ),  $g(y)$  is a Gaussian function. A larger value of  $\gamma$  implies a stronger power-law tail for  $y \gg 1$ .

If we had allowed the boundary condition  $g'(0)$  to be a nonzero constant, the resulting solutions for  $g(y)$  would have been asymmetric about  $k_{\parallel} = 0$ . Naïvely, these solutions could be considered to be applicable to the relevant case of more power in outward propagating fluctuations than in inward propagating fluctuations. However, the solutions exhibit unphysically negative values of  $g$  throughout most of the “weaker” half of the distribution, and thus are probably inapplicable.

## REFERENCES

- Abraham-Shrauner, B., & Feldman, W. C. 1977, *J. Geophys. Res.*, 82, 618
- Ambrosiano, J., Matthaeus, W. H., Goldstein, M. L., & Plante, D. 1988, *J. Geophys. Res.*, 93, 14383
- Axford, W. I., & McKenzie, J. F. 1992, in *Solar Wind Seven*, ed. E. Marsch & R. Schwenn (New York: Pergamon), 1
- Bale, S. D., Kellogg, P. J., Larson, D. E., Lin, R. P., Goetz, K., & Lepping, R. P. 1998, *Geophys. Res. Lett.*, 25, 2929
- Bale, S. D., Hull, A., Larson, D. E., Lin, R. P., Muschietti, L., Kellogg, P. J., Goetz, K., & Monson, S. J. 2002, *ApJ*, 575, L25
- Banaszkiewicz, M., Axford, W. I., & McKenzie, J. F. 1998, *A&A*, 337, 940
- Banerjee, D., Teriaca, L., Doyle, J. G., & Wilhelm, K. 1998, *A&A*, 339, 208
- Barnes, A. 1968, *ApJ*, 154, 751
- Batchelor, G. K. 1953, *Theory of Homogeneous Turbulence* (Cambridge: Cambridge Univ. Press)
- Bernstein, I. B. 1958, *Phys. Rev.*, 109, 10
- Bernstein, I. B., Greene, J. M., & Kruskal, M. D. 1957, *Phys. Rev.*, 108, 546
- Bhattacharjee, A., & Ng, C. S. 2001, *ApJ*, 548, 318
- Biglari, H., & Diamond, P. H. 1989, *Physica D*, 37, 206

- Brambilla, M. 1998, *Kinetic Theory of Plasma Waves: Homogeneous Plasmas* (Oxford: Clarendon)
- Cairns, I. H. 1987, *J. Geophys. Res.*, 92, 2315
- Chae, J., Schühle, U., & Lemaire, P. 1998, *ApJ*, 505, 957
- Chandrasekhar, S. 1943, *Rev. Mod. Phys.*, 15, 1
- Chen, L.-J., & Parks, G. K. 2001, arXiv.org preprint, physics/0103020
- Chen, L.-J., & Parks, G. K. 2002, *Geophys. Res. Lett.*, 29 (9), 1331, 10.1029/2001GL013385
- Cho, J., Lazarian, A., & Vishniac, E. T. 2002, *ApJ*, 564, 291
- Cranmer, S. R. 1998, *ApJ*, 508, 925
- Cranmer, S. R. 2000, *ApJ*, 532, 1197
- Cranmer, S. R. 2001, *J. Geophys. Res.*, 106, 24937
- Cranmer, S. R. 2002, *Space Sci. Rev.*, 101, 229
- Cranmer, S. R., Field, G. B., & Kohl, J. L. 1999a, *ApJ*, 518, 937
- Cranmer, S. R., et al. 1999b, *ApJ*, 511, 481
- Davidson, R. C. 1983, in *Basic Plasma Physics I*, ed. A. A. Galeev & R. N. Sudan (Amsterdam: North Holland), 519
- Dmitruk, Matthaueus, W. H., Milano, L. J., Oughton, S., Zank, G. P., & Mullan, D. J. 2002, *ApJ*, 575, 571
- Dmitruk, P., Milano, L. J., & Matthaueus, W. H. 2001, *ApJ*, 548, 482
- Dobrowolny, M., & Torricelli-Ciamponi, G. 1985, *A&A*, 142, 404
- Doschek, G. A., Feldman, U., Laming, J. M., Schühle, U., & Wilhelm, K. 2001, *ApJ*, 546, 559
- Drake, J. F., Swisdak, M., Cattell, C., Shay, M. A., Rogers, B. N., & Zeiler, A. 2003, *Science*, 299, 873
- Dum, C. T. 1990, *J. Geophys. Res.*, 95, 8095
- Dupree, T. H. 1982, *Phys. Fluids*, 25, 277
- Dusenbery, P. B., & Hollweg, J. V. 1981, *J. Geophys. Res.*, 86, 153
- Eichler, D. 1979, *ApJ*, 229, 413
- Ergun, R. E., Carlson, C. W., McFadden, J. P., Mozer, F. S., Muschietti, L., Roth, I., & Strangeway, R. J. 1998, *Phys. Rev. Lett.*, 81, 826
- Ergun, R. E., Carlson, C. W., Muschietti, L., Roth, I., & McFadden, J. P. 1999, *Nonlin. Proc. Geophys.*, 6, 187
- Esser, R., & Habbal, S. R. 1995, *Geophys. Res. Lett.*, 22, 2661
- Esser, R., Fineschi, S., Dobrzycka, D., Habbal, S. R., Edgar, R. J., Raymond, J. C., Kohl, J. L., & Guhathakurta, M. 1999, *ApJ*, 510, L63
- Franz, J. R., Kintner, P. M., Seyler, C. E., Pickett, J. S., & Scudder, J. D. 2000, *Geophys. Res. Lett.*, 27, 169
- Fried, B. D., & Conte, S. D. 1961, *The Plasma Dispersion Function: The Hilbert Transform of the Gaussian* (New York: Academic)
- Galinsky, V. L., & Shevchenko, V. I. 2000, *Phys. Rev. Lett.*, 85, 90
- Giordano, S., Antonucci, E., Noci, G., Romoli, M., & Kohl, J. L. 2000, *ApJ*, 531, L79
- Goldreich, P., & Sridhar, S. 1995, *ApJ*, 438, 763
- Goldreich, P., & Sridhar, S. 1997, *ApJ*, 485, 680
- Goldstein, M. L., Roberts, D. A., & Matthaueus, W. H. 1995, *ARA&A*, 33, 283
- Gomberoff, L., Gratton, F. T., & Gnani, G. 1996, *J. Geophys. Res.*, 101, 15661
- Grall, R. R., Coles, W. A., Spangler, S. R., Sakurai, T., & Harmon, J. K. 1997, *J. Geophys. Res.*, 102, 263
- Hasegawa, A. 1976, *J. Geophys. Res.*, 81, 5083
- Hollweg, J. V. 1973, *ApJ*, 181, 547
- Hollweg, J. V. 1978, *Rev. Geophys. Space Phys.*, 16, 689
- Hollweg, J. V. 1986, *J. Geophys. Res.*, 91, 4111
- Hollweg, J. V. 1999a, *J. Geophys. Res.*, 104, 14811
- Hollweg, J. V. 1999b, *J. Geophys. Res.*, 104, 24781
- Hollweg, J. V. 2000, *J. Geophys. Res.*, 105, 7573
- Hollweg, J. V., & Isenberg, P. A. 2002, *J. Geophys. Res.*, 107 (A7), 1147, 10.1029/2001JA000270
- Hollweg, J. V., & Markovskii, S. A. 2002, *J. Geophys. Res.*, 107 (A6), 1080, 10.1029/2001JA000205
- Hollweg, J. V., & Turner, J. M. 1978, *J. Geophys. Res.*, 83, 97
- Isenberg, P. A. 1984, *J. Geophys. Res.*, 89, 2133
- Isenberg, P. A. 2001, *J. Geophys. Res.*, 106, 29249
- Isenberg, P. A. 2003, *J. Geophys. Res.*, in press
- Isenberg, P. A., & Hollweg, J. V. 1983, *J. Geophys. Res.*, 88, 3923
- Jackson, J. D. 1975, *Classical Electrodynamics*, 2nd ed. (New York: Wiley)
- Jacques, S. A. 1977, *ApJ*, 215, 942
- Kaghashvili, E. K., & Esser, R. 2000, *ApJ*, 539, 463
- Kohl, J. L., Strachan, L., & Gardner, L. D. 1996, *ApJ*, 465, L141
- Kohl, J. L., et al. 1997, *Sol. Phys.*, 175, 613
- Kohl, J. L., et al. 1998, *ApJ*, 501, L127
- Kohl, J. L., et al. 1999, *ApJ*, 510, L59
- Kolmogorov, A. N. 1941, *Dokl. Akad. Nauk SSSR*, 30, 301
- Kraichnan, R. H. 1965, *Phys. Fluids*, 8, 1385

- Krasovsky, V. L., Matsumoto, H., & Omura, Y. 1999, *Phys. Scr*, 60, 438
- Krauss-Varban, D., Omid, N., & Quest, K. B. 1994, *J. Geophys. Res.*, 99, 5987
- Lazarian, A., & Vishniac, E. T. 1999, *ApJ*, 517, 700
- Leamon, R. J., Matthaeus, W. H., Smith, C. W., Zank, G. P., Mullan, D. J., & Oughton, S. 2000, *ApJ*, 537, 1054
- Leamon, R. J., Smith, C. W., Ness, N. F., Matthaeus, W. H., & Wong, H. K. 1998, *J. Geophys. Res.*, 103, 4775
- Leamon, R. J., Smith, C. W., Ness, N. F., & Wong, H. K. 1999, *J. Geophys. Res.*, 104, 22331
- Lee, L. C., & Wu, B. H. 2000, *ApJ*, 535, 1014
- Leer, E., Holzer, T. E., & Flå, T. 1982, *Space Sci. Rev.*, 33, 161
- Leubner, M. P. 2001, in *Recent Insights into the Physics of the Sun and Heliosphere*, IAU Symp. 203, ed. P. Brekke, B. Fleck, & J. Gurman (San Francisco: ASP), 544
- Leith, C. E. 1967, *Phys. Fluids*, 10, 1409
- Li, X. 1999, *J. Geophys. Res.*, 104, 19773
- Li, X., & Habbal, S. R. 2001, *J. Geophys. Res.*, 106, 10669
- Li, X., Habbal, S. R., Hollweg, J. V., & Esser, R. 1999, *J. Geophys. Res.*, 104, 2521
- Lysak, R. L., & Lotko, W. 1996, *J. Geophys. Res.*, 101, 5085
- Mariska, J. T., Feldman, U., & Doschek, G. A. 1978, *ApJ*, 226, 698
- Markovskii, S. A. 2001, *ApJ*, 557, 337
- Markovskii, S. A., & Hollweg, J. V. 2002, *Geophys. Res. Lett.*, 29 (17), 1843, 10.1029/2002GL015189
- Maron, J., & Goldreich, P. 2001, *ApJ*, 554, 1175
- Marsch, E. 1991, in *Physics of the Inner Heliosphere*, Vol. II, ed. R. Schwenn & E. Marsch (Heidelberg: Springer-Verlag), 45
- Marsch, E., Goertz, C. K., & Richter, K. 1982, *J. Geophys. Res.*, 87, 5030
- Marsch, E., & Tu, C.-Y. 1997, *A&A*, 319, L17
- Marsch, E., & Tu, C.-Y. 2001, *J. Geophys. Res.*, 106, 227
- Marsch, E., Tu, C.-Y., & Rosenbauer, H. 1996, *Ann. Geophysicae*, 14, 259
- Matsumoto, H., Kojima, H., Miyatake, T., Omura, Y., Okada, M., Nagano, I., & Tsutsui, M. 1994, *Geophys. Res. Lett.*, 21, 2915
- Matthaeus, W. H., Dmitruk, P., Oughton, S., Mullan, D., & Zank, G. P. 2003a, in *Solar Wind Ten*, ed. M. Velli & R. Bruno (Woodbury, NY: AIP), in press
- Matthaeus, W. H., Ghosh, S., Oughton, S., & Roberts, D. A. 1996, *J. Geophys. Res.*, 101, 7619
- Matthaeus, W. H., & Lamkin, S. L. 1986, *Phys. Fluids*, 29, 2513
- Matthaeus, W. H., Mullan, D., Dmitruk, P., Milano, L., & Oughton, S. 2003b, *Nonlin. Proc. Geophys.*, 10, 93
- Matthaeus, W. H., Zank, G. P., Oughton, S., Mullan, D. J., & Dmitruk, P. 1999, *ApJ*, 523, L93
- McKenzie, J. F., Banaszekiewicz, M., & Axford, W. I. 1995, *A&A*, 303, L45
- Medvedev, M. V. 2000, *ApJ*, 541, 811
- Melrose, D. B. 1986, *Instabilities in Space and Laboratory Plasmas* (Cambridge: Cambridge Univ. Press)
- Melrose, D. B., & Goldman, M. V. 1987, *Sol. Phys.*, 107, 329
- Miller, J. A., LaRosa, T. N., & Moore, R. L. 1996, *ApJ*, 461, 445
- Montgomery, D. 1982, *Phys. Scr*, T2/1, 83
- Moran, T. G. 2002, *BAAS*, 34, 790 (abstract 88.05)
- Mottez, F. 2001, *Ap&SS*, 277, 59
- Noci, G., et al. 1997, *Adv. Space Res.*, 20 (12), 2219
- Obukhov, A. M. 1941, *Dokl. Akad. Nauk SSSR*, 32, 19
- Olbert, S. 1969, in *Physics of the Magnetosphere*, ed. R. L. Carovillano, J. F. McClay, & H. R. Radoski (Dordrecht: Reidel), 641
- Olsen, E. L., & Leer, E. 1996, *ApJ*, 462, 982
- Omura, Y., Kojima, H., Umeda, T., & Matsumoto, H. 2001, *Ap&SS*, 277, 45
- Pao, Y.-H. 1965, *Phys. Fluids*, 8, 1063
- Parker, E. N. 1991, *ApJ*, 372, 719
- Phillips, J. L., Feldman, W. C., Gosling, J. T., & Scime, E. E. 1995, *Adv. Space Res.*, 16 (9), 95
- Poppe, G. P. M., & Wijers, C. M. J. 1990, *ACM Trans. Math. Soft.*, 16, 38
- Press, W. H., Teukolsky, S. A., Vetterling, W. T., & Flannery, B. P. 1992, *Numerical Recipes in Fortran: The Art of Scientific Computing* (Cambridge: Cambridge Univ. Press)
- Priest, E. R., Foley, C. R., Heyvaerts, J., Arber, T. D., Mackay, D., Culhane, J. L., & Acton, L. W. 2000, *ApJ*, 539, 1002
- Quataert, E. 1998, *ApJ*, 500, 978
- Quataert, E., & Gruzinov, A. 1999, *ApJ*, 520, 248
- Richardson, J. D., Paularena, K. I., Lazarus, A. J., & Belcher, J. W. 1995, *Geophys. Res. Lett.*, 22, 325
- Roberts, B. 2000, *Sol. Phys.*, 193, 139
- Roberts, D. A., Goldstein, M. L., Matthaeus, W. H., & Ghosh, S. 1992, *J. Geophys. Res.*, 97, 17115
- Schwartz, S. J., Feldman, W. C., & Gary, S. P. 1981, *J. Geophys. Res.*, 86, 541

- Schwartz, S. J., and Marsch, E. 1983, *J. Geophys. Res.*, 88, 9919
- Scudder, J. D. 1992, *ApJ*, 398, 319
- Shebalin, J. V., Matthaeus, W. H., & Montgomery, D. 1983, *J. Plasma Phys.*, 29, 525
- Shukla, P. K., Bingham, R., McKenzie, J. F., & Axford, W. I. 1999, *Sol. Phys.*, 186, 61
- Song, L.-T. 1996, *Chinese Astron. & Astrophys.*, 20, 221
- Spangler, S. R. 1991, *ApJ*, 376, 540
- Spangler, S. R. 1997, in *Nonlinear Waves and Chaos in Space Plasmas*, ed. T. Hada & H. Matsumoto (Tokyo: Terra Sci. Pub.), 171
- Spangler, S. R. 2002, *ApJ*, 576, 997
- Spitzer, L., Jr. 1962, *Physics of Fully Ionized Gases*, 2nd ed. (New York: Wiley)
- Stasiewicz, K., et al. 2000, *Space Sci. Rev.*, 92, 423
- Stawicki, O., Gary, S. P., & Li, H. 2001, *J. Geophys. Res.*, 106, 8273
- Stéfant, R. J. 1970, *Phys. Fluids*, 13, 440
- Stix, T. H. 1992, *Waves in Plasmas* (New York: AIP)
- Strauss, H. R. 1976, *Phys. Fluids*, 19, 134
- Tanaka, M., Sato, T., & Hasegawa, A. 1987, *Geophys. Res. Lett.*, 14, 868
- Tanaka, M., Sato, T., & Hasegawa, A. 1989, *Phys. Fluids B*, 1, 325
- Thompson, J. R. 1971, *Phys. Fluids*, 14, 1532
- Toichi, T. 1971, *Sol. Phys.*, 18, 150
- Townsend, A. A. 1951, *Proc. Roy. Soc. A*, 208, 534
- Tu, C.-Y. 1987, *Sol. Phys.*, 109, 149
- Tu, C.-Y. 1988, *J. Geophys. Res.*, 93, 7
- Tu, C.-Y., & Marsch, E. 1995, *Space Sci. Rev.*, 73, 1
- Tu, C.-Y., & Marsch, E. 1997, *Sol. Phys.*, 171, 363
- Tu, C.-Y., & Marsch, E. 2001, *J. Geophys. Res.*, 106, 8233
- Tu, C.-Y., & Marsch, E. 2002, *J. Geophys. Res.*, 107 (A9), 1249, 10.1029/2001JA000150
- Tu, C.-Y., Marsch, E., & Rosenbauer, H. 1996, *Ann. Geophysicae*, 14, 270
- Tu, C.-Y., Pu, Z.-Y., & Wei, F.-S. 1984, *J. Geophys. Res.*, 89, 9695
- Turikov, V. A. 1984, *Phys. Scr*, 30, 73
- van Ballegooijen, A. A. 1986, *ApJ*, 311, 1001
- Vasquez, B. J., Markovskii, S. A., & Hollweg, J. V. 2002, *Eos Trans. AGU*, 83 (47), Fall Meet. Suppl., F1156 (abstract SH12A-0408)
- Vocks, C., & Marsch, E. 2002, *ApJ*, 568, 1030
- Voitenko, Y., & Goossens, M. 2002, *Sol. Phys.*, 209, 37
- Withbroe, G. L., Kohl, J. L., Weiser, H., & Munro, R. H. 1982, *Space Sci. Rev.*, 33, 17
- Zank, G. P., Matthaeus, W. H., & Smith, C. W. 1996, *J. Geophys. Res.*, 101, 17093
- Zhou, Y., & Matthaeus, W. H. 1990, *J. Geophys. Res.*, 95, 14881

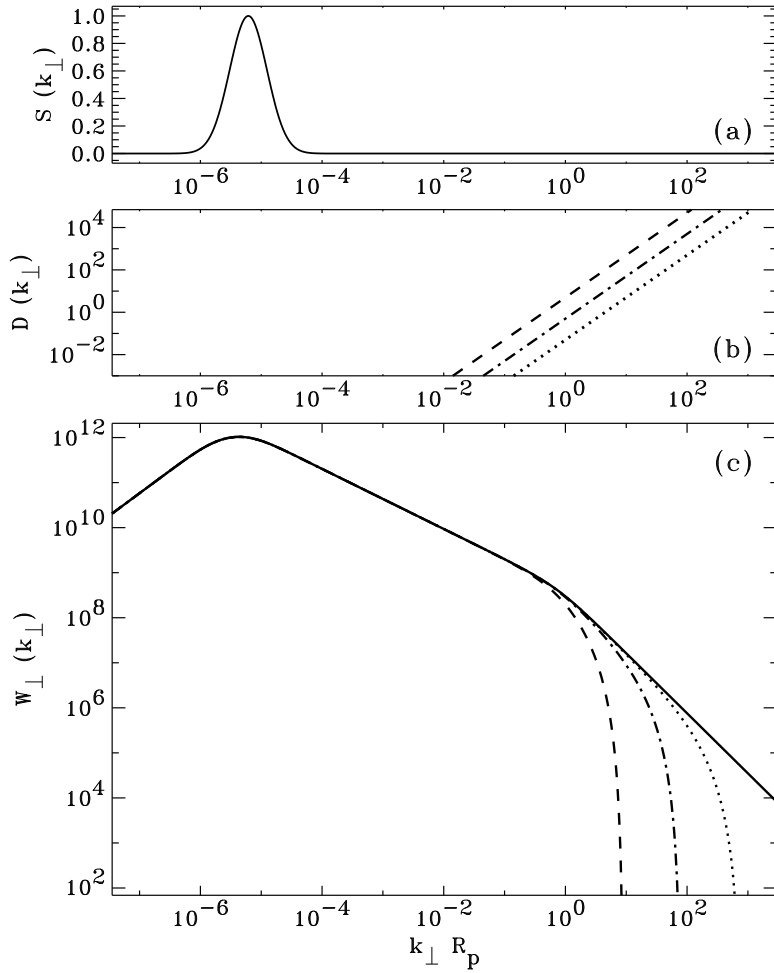


Fig. 1.— Representative solutions for the dominant perpendicular cascade at  $r = 2 R_{\odot}$ : (a) outer-scale energy source function  $S(k_{\perp})$ , normalized to its maximum value; (b) dissipation rate  $D(k_{\perp}) = D_0(k_{\perp}R_p)^2$ , where  $D_0 = 0.05 \text{ s}^{-1}$  (dotted line),  $0.5 \text{ s}^{-1}$  (dot-dashed line), and  $5 \text{ s}^{-1}$  (dashed line); (c) time-steady reduced power spectrum  $W_{\perp}(k_{\perp})$  for the three dissipation rates above, and for zero dissipation (solid line). The proton gyroradius  $R_p$  at this radius in the extended corona is assumed to be equal to 0.024 km.

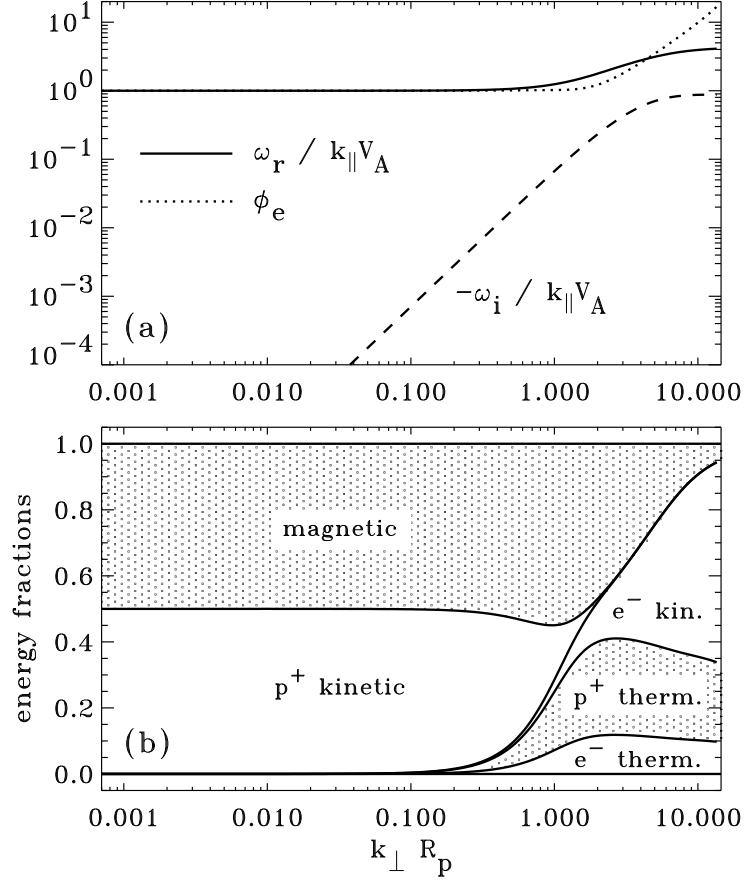


Fig. 2.— Dispersion and energy density properties of kinetic Alfvén waves as a function of  $k_{\perp}$ : (a) real (*solid line*) and imaginary (*dashed line*) parts of the wave frequency, scaled by the MHD Alfvén frequency, and the dimensionless energy parameter  $\phi_e$  (*dotted line*); (b) linearized energy density fractions—expressed as areas—from top to bottom: magnetic field, proton kinetic (i.e., velocity perturbation), electron kinetic, proton thermal (i.e., density perturbation), and electron thermal. All curves correspond to a constant value of  $k_{\parallel} V_A / \Omega_p = 10^{-3}$ .

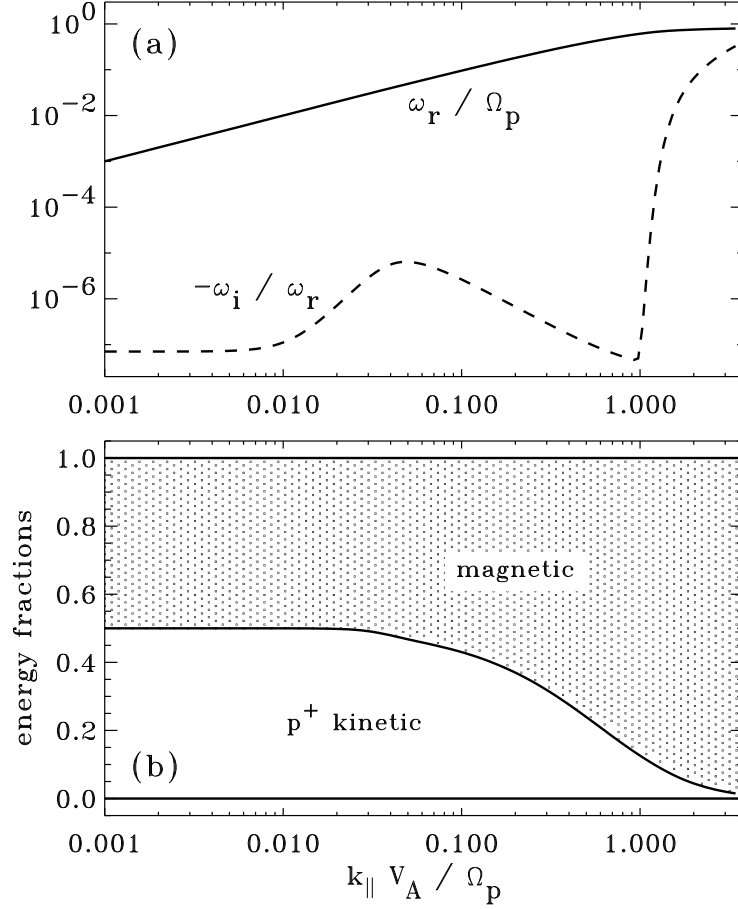


Fig. 3.— Dispersion and energy density properties of nearly parallel-propagating Alfvén waves (approaching ion cyclotron resonance) as a function of  $k_{\parallel}$ . Curves in (a) and areas in (b) are similar to those in Figure 2, but the normalizations in (a) are different (*see plot annotations*). All curves correspond to a constant value of  $k_{\perp} R_p = 10^{-3}$ .

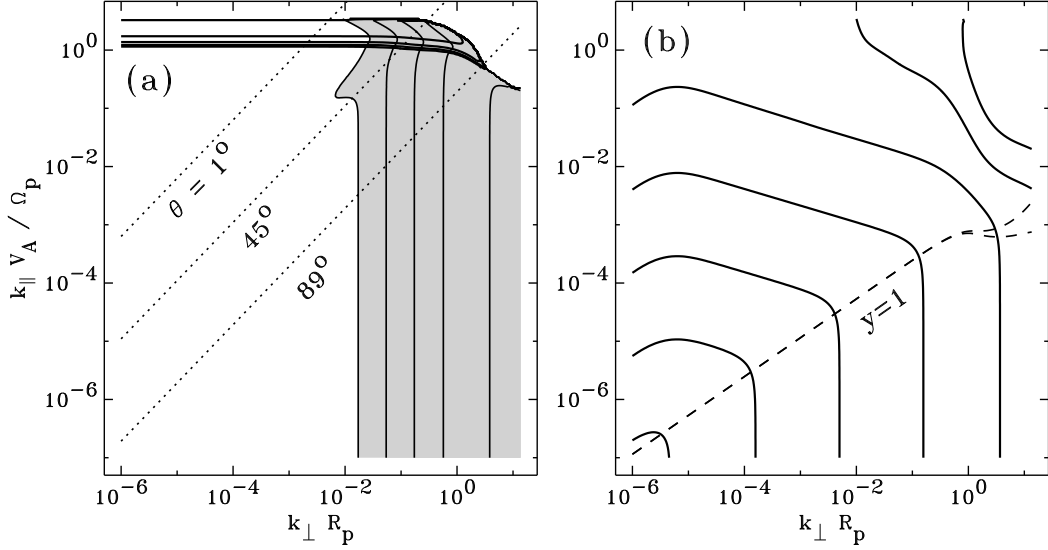


Fig. 4.— (a) Dimensionless damping rates  $|\omega_{i,s}/\omega_r|$  for protons (*unfilled contours*) and electrons (*filled contours*) plotted one per decade between  $9 \times 10^{-5}$  and  $9 \times 10^{-1}$  times the maximum values of  $|\omega_{i,s}/\omega_r|$  of 0.329 (protons) and 0.231 (electrons). Both sets of contours go from low to high values with increasing wavenumber. Dotted lines show contours in  $\theta$ , the angle between  $\mathbf{B}_0$  and  $\mathbf{k}$ . (b) Contours of  $W(\mathbf{k})$ , plotted one per  $10^5$  between  $10^{10}$  and  $10^{40} \text{ cm}^5 \text{ s}^{-2}$  (*solid lines*) with the largest values at lower left. Critical balance curves also plotted for both the undamped (*upper dashed line*) and damped (*lower dashed line*) calculations of  $W_{\perp}(k_{\perp})$ .

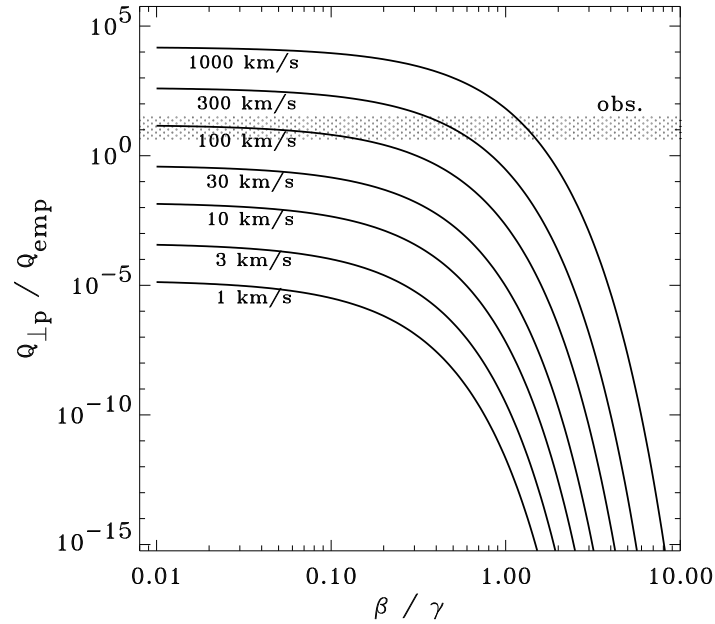


Fig. 5.— Perpendicular proton heating rates, in units of a fiducial empirical rate  $Q_{\text{emp}}$  (see text), plotted versus  $\beta/\gamma$  for a range of total wave amplitudes  $(\delta U/\rho)^{1/2}$  (see labels on each curve). The hashed region denotes empirical rates from Li et al. (1999).

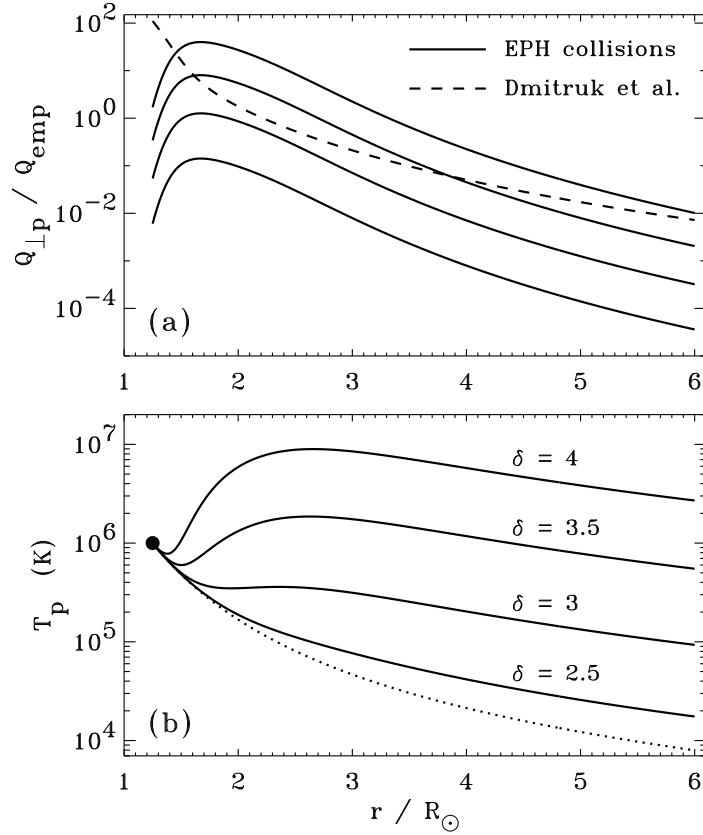


Fig. 6.— (a) Normalized proton heating rates plotted versus heliocentric radius, both for the turbulent cascade rate of Dmitruk et al. (2002) (*dashed line*) and for the derived ion/EPH diffusion coefficient (*solid lines*). From bottom to top,  $\delta = 2.5, 3, 3.5, 4$ . (b) Perpendicular proton temperatures derived with the ion/EPH heating rates plotted in (a) (*solid lines*), and with no imposed heating (i.e., adiabatic cooling only; *dotted line*).

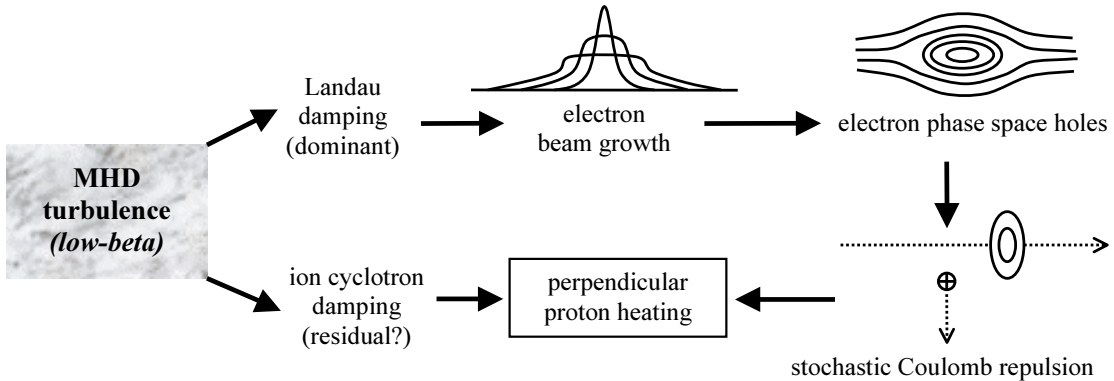


Fig. 7.— Schematic representation of the major physical processes discussed in this paper. The relative amount of turbulent dissipation that directly heats protons and electrons depends, among other factors, on the ratio  $\beta/\gamma$ . The nonlinear development of parallel electron beams into phase-space holes that can interact with protons is also illustrated.